Faculty of Science & Technology

Assessing the Significance of Aspect on Multi-Decadal Changes in Glacier Thickness of Marine Terminating Glaciers on the Antarctic Peninsula

A dissertation submitted as part of the requirement for the BSc Environmental Science

Evangeline Rowe

S5319838

5th May 2023

ALS Marking Guidelines

Abstract

Glaciers currently account for 60% of the ice mass lost in Antarctica, with Antarctic Peninsula glaciers having a potential contribution of 54mm to global sea level rise (Meier et al. 2007; Huber et al. 2017). Furthermore, existing literature increasingly recognises the spatial distribution of glacier mass loss on the Antarctic Peninsula, attributed to various internal and external processes (Cook 2014). However, the significance of aspect has yet to be investigated at a local scale for glaciers at extreme latitudes. Subsequently this research investigates the significance of aspect on observed multi-decadal changes in glacier thickness of marine-terminating glaciers on the Antarctic Peninsula. Two marine-terminating glaciers of opposing aspect, Leonardo westward facing, and Diplock eastward, were identified based on the availability of historic aerial photography. Digital Elevation Models (DEMs) were produced from archived film photography collected in 1957 by the British Antarctic Survey, and recent 2009/2016 digital photography collected by NASA's operation Icebridge. A limitation of using this method is the lack of high spatial resolution geographic reference data. Subsequently DEMs for Leonardo, 1957 and 2009, have a RMSE of 5.13m and 6.98m respectively, and Diplock 1957 and 2016, 7.50m and 7.54m. The findings of this investigation support existing research, with observed thinning on the west coast from increased carving and shrinking of east coast glaciers following terminus retreat (Davies et al. 2012; Seehaus et al. 2018). To conclude, aspect was found to be significant locally, in addition to playing a role in regional changes. Furthermore, these findings suggest that as east coast tributary glaciers decelerate following ice shelf collapse, the contribution of westward marine-terminating glaciers to mass loss are expected to outweigh that lost on the east, because of persistent warm waters and increasing air temperatures driving ablation (Cook 2014; Seehaus et al. 2018; Turner et al. 2020). However, due to the complexities of external processes, more work must be done to investigate the role of aspect on regional mass balance.

Acknowledgements

I would like to thank the following people for their contribution, academically, professionally, and personally to the completion of this research project.

Firstly, my dissertation supervisor, Andrew Ford, for his guidance and encouragement throughout this project, and for his many wise words.

Harry Manley, Demonstrator in Geoinformatics, for his help throughout my time at Bournemouth University in modules such as Geographic Information systems, and Remote Sensing, which taught me the skills necessary to complete this research project.

Dr Iain Green, BSc Environmental Science Programme Leader, for his support and encouragement over the past three years.

The British Antarctic Survey Mapping and Geographic Information Centre for their assistance in providing geospatial information regarding archived aerial film photography.

Ildiko Balogh, Assisted Learning and Support Specialist Tutor at Bournemouth University, for her unrivalled support this past year in helping me manage and prioritise my time, write concisely, and have more confidence in my abilities.

My family in supporting me in going back to education and following my dreams.

Finally, my partner, Edward Nancarrow, for his help with statistical analysis in addition to putting up with my one-way glacier dialog for the past few months, and for always encouraging and believing in me, without which I would not be completing this degree.

Table of Contents

1.0 Introduction and literature review

1.1 Glacier Mass Balance

Terrestrial ice mass (TIM), otherwise known as Land Ice, covers 10% of the earth surface and stores approximately 33 million km^3 freshwater, equivalent to 70m of global sea level rise (Benn and Evans 1998). Glaciers are the smallest TIM covering an area of ~225,500km^2, found both at extreme latitudes, and at high-altitude mid-latitudes where temperatures are consistently low (Figure 1). Glaciers are formed by the accumulation of snow, which is compressed into firn, and glacial ice via the process of densification (Oraschewski and Grinsted 2022). They flow plastically under gravity and deform internally because of their mass, exerting erosional forces onto the bed beneath them (Parks 2022). Mass is accumulated within the accumulation zone, and lost, or ablated downslope in the ablation zone (Figure 2) (Meier 2022). Ablation occurs via melting, carving into icebergs, and sublimation, common in arid regions such as Antarctica (Meier 2022). Mass balance is calculated as the difference between accumulation and ablation over time and varies in response to environmental conditions and is subsequently a valuable indicator of climate change (Kurtz 2013).

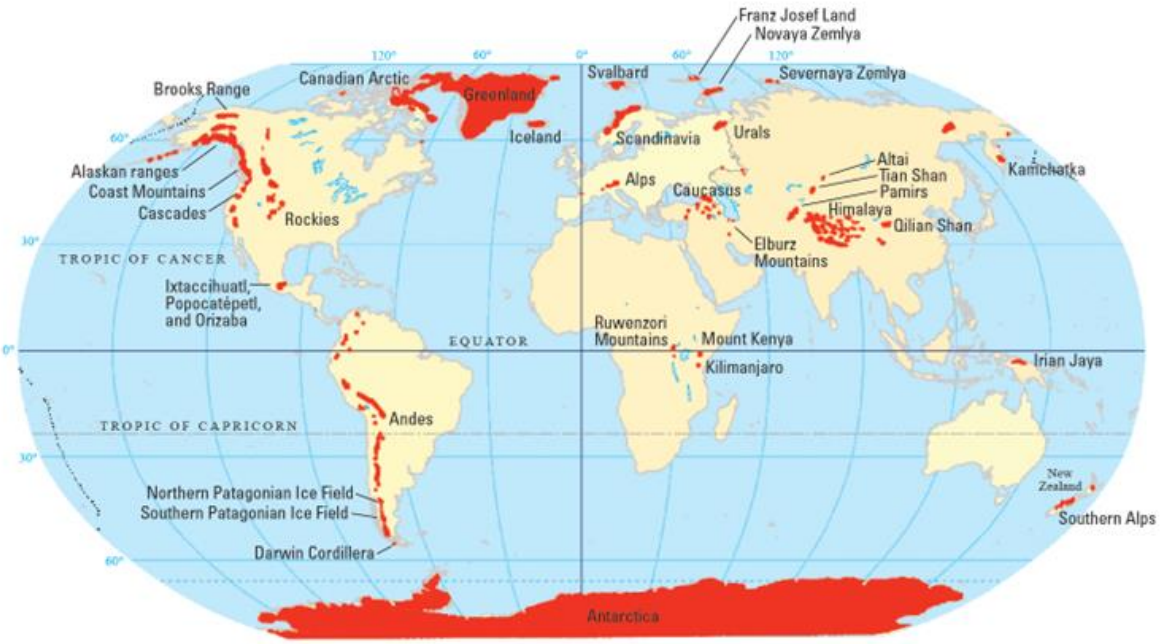

Figure 1. Geographic distribution of terrestrial ice mass obtained from USGS Satellite image atlas of glacier of the world (Williams and Ferrigno 2005).

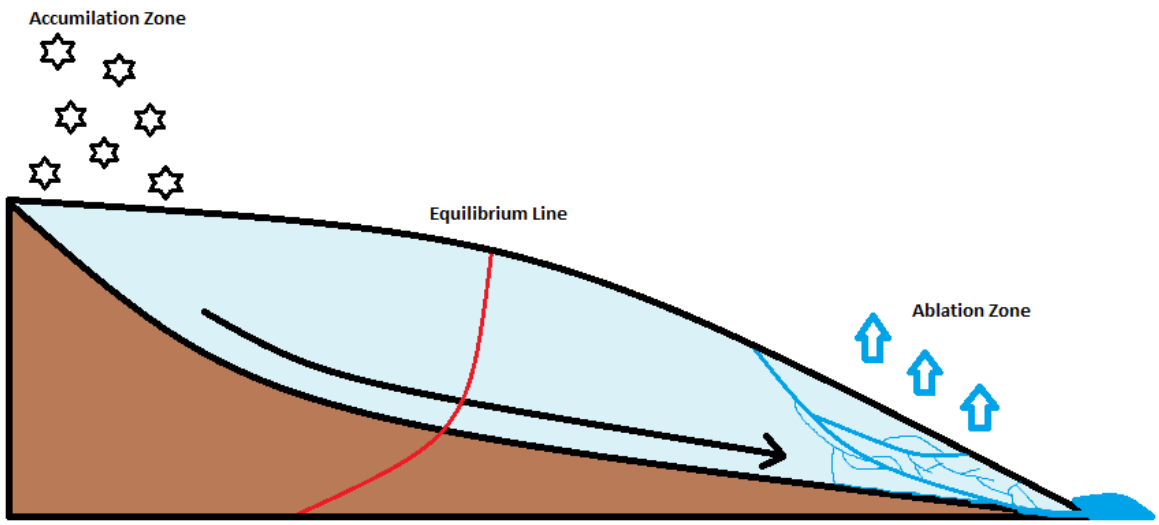

Figure 2. A hypothetical glacier, black arrow shows the direction of flow from the accumulation zone, past the equilibrium line (red) where accumulation is equal to ablation, downslope to the ablation zone.

There are various indicative measures of mass balance, one of which is the Equilibrium Line Altitude (ELA) (Hubbard and Glasser 2005; Johnson et al. 2020). The ELA is the point at which there is no net mass gain or loss, as shown in Figure 2, and varies seasonally due to winter precipitation and summer melt (Hubbard and Glasser 2005; Nesje 2014). When annual mass balance is negative, the ELA rises, and when positive, ELA falls (Nesje 2014). Various approaches exist for measuring ELA, consequential of the complex relationship between mass balance and altitude (Osmaston 2005; Braithwaite and Raper 2009). Braithwaite and Raper (2009) argue the best approach is the balanced-budget ELA. In their study of 94 glaciers, they found this measure to be strongly correlated to median glacier altitude, and as a result, mass balance can be accurately extrapolated (Figure 3) (Braithwaite and Raper 2009; Braithwaite 2017). However, for glaciers with unknown mass balance, different approaches produce varying results such that it is difficult to accurately estimate mass balance from ELA, and as a result, this measure lacks precision (Braithwaite 2017).

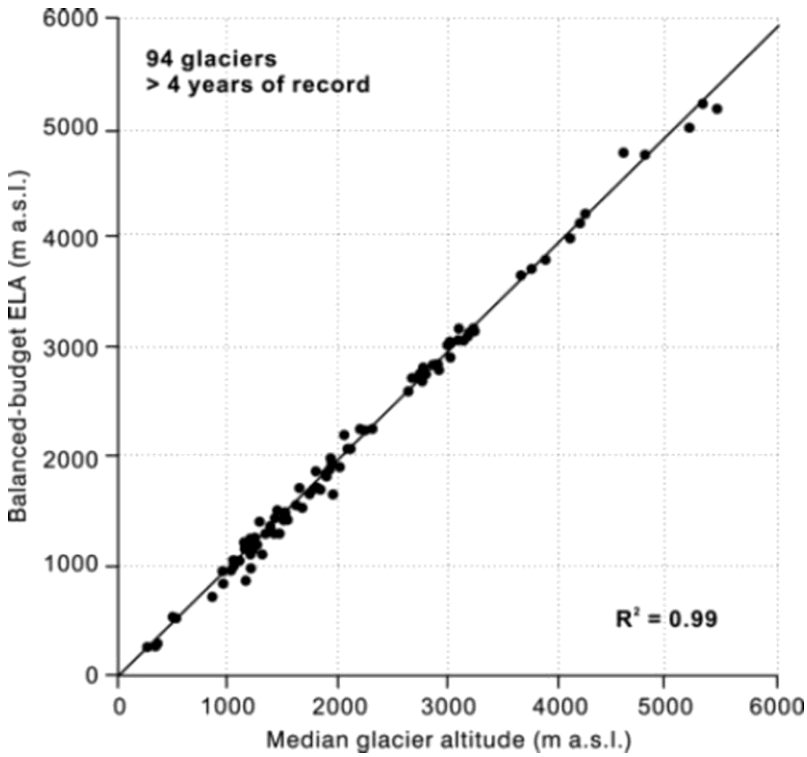

Figure 3. The relationship between balanced-budget ELA and median glacier altitude obtained from Braithwaite and Raper 2009.

Glacier extent is another measure indicative of mass balance, calculated as the total area of glacier surface, and can be obtained from indirect methods (Figure 4). A benefit of using indirect methods, such as aerial photography, is the availability of historical photographs which enabled Thompson et al. (2009) to produce a 92-year record of Kilimanjaro's glacier extent. However, extent is greatly affected by topography and thus alone, lacks precision. Additionally, surface area is not a measure of volume (Davies 2015).

The volume of a glacier can be calculated by measuring the elevation and extent, and therefore volumetric change be estimated by subtracting the surface elevation and extent of a glacier from different periods (Kaser et al. 2003; Hubbard and Glasser 2005). Elevation is presented as a Digital Elevation Model (DEM), and varies in its accuracy and precision, dependant the source data and methodology as discussed in section 1.2 (VanLooy et al. 2006). The most accurate source data is those with the highest spatial resolution, and most precise mass balance calculations, obtained by combining different measures.

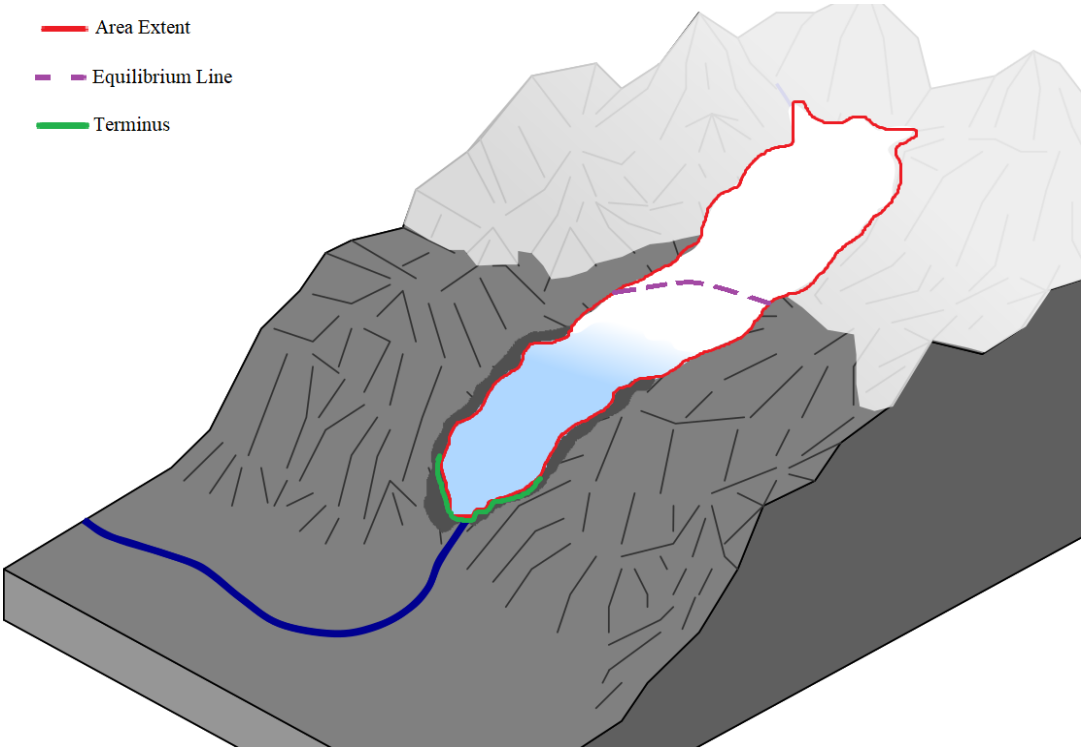

Figure 4. Hypothetical valley glacier showing different observational measures indicative of mass balance including Glacier Extent, Equilibrium Line Altitude (Figure 2) and Terminus position. Where the blue line represents a meltwater stream.

As summarised in Table 1, ELA and extent lack precision as they are indicators rather than volumetric measures of mass balance. However, when combined with measures such as elevation, their accuracy and precision is improved. Since ELA and elevation are both a measure of height, the best measure of mass balance is a combination of elevation and extent.

Table 1. Summary of the strengths, weaknesses, accuracy, and precision of measures of glacial mass balance discussed in section 1.1.

Measure	Strengths	Weaknesses	Accuracy	Precision
ELA	Altitude is a strong indicator of mass balance. Can accurately estimate mass balance after a few years of records (Braithwaite 2017).	Different approaches produce differing results. Lacks accuracy for glaciers with no mass balance record (Braithwaite 2017).	Low	Low

Extent	Indicator of mass balance. Can be obtained from indirect methods to produce long-term records (Thompson et al. 2009).	Greatly affected by topography. Lacks volumetric data.	Medium	Low
Elevation	DEMs show volumetric change across glacier (Hubbard and Glasser 2005). Global, regional, and local glacial monitoring.	DEM quality is dependent upon source data (VanLooy et al. 2006).	Medium - High	Medium - High

1.2 Methods of Measuring Elevation

Elevation can be measured using a variety of direct and indirect methods. Glaciological mass balance is measured directly, in the field, and Geodetic mass balance measured indirectly, from a distance (Knight 1999). DEMs are produced from both direct and indirect measures of elevation such as Staking, GNSS Surveys, InSAR, LiDAR and Passive imagery, each of which are discussed in the following section and summarised in Table 6.

1.2.1 Direct: Staking and GNSS Surveys

Traditionally mass balance was measured directly by staking out the glacier surface, providing points from which elevation can be measured (Davies 2020a). Louis Agassiz was the first to conduct a glaciological study using stakes in their 1847 study of the Lower Aare Glacier, Switzerland (Steiner et al. 2007). Whilst still used today, staking lacks the accuracy and precision offered by more sophisticated direct methods such as Global Navigation Satellite System (GNSS) surveys (Correa-Muños and Cerón-Calderón 2018). GNSS surveys measure elevation from point measurements collected on the glacier surface, as opposed to measuring change in elevation relative to that of stakes. However, this technology is expensive and in general direct measures are very labour intensive and thus, only suitable for measuring individual glaciers (Davies 2015). Additionally, field work is usually only conducted in the summer due to weather conditions, as a result mass balance is interpolated from seasonal observations (Volksen and Mayer 2016). Thompson et al. (2009), found that

using averages based on interpolated results led to the overestimation of loss by thinning and underestimation of loss by shrinking. Due to these limitations, direct measurements have only been obtained for <0.3% of glaciers worldwide (Li et al. 2021).

1.2.2 Indirect: InSAR and LiDAR

New technologies have enabled us to measure elevation using airborne and satellite-based systems. Interferometric Synthetic Aperture Radar (InSAR) are active systems, which emit their own energy in the form of microwaves to monitor changes on the earth's surface (National Aeronautics and Space Administration (NASA) 2023). Subsequently, a huge advantage of InSAR is that it is not reliant upon a passive light source and is therefore unaffected by time of day, seasonality, or cloud cover. Additionally, different frequencies and wavelengths emitted respond to different characteristics of the earth's surface, with some wavelengths able to penetrate snow and ice (NASA 2023). Therefore, InSAR can be used to quantify surface topography, providing additional information regarding glacial bed morphology (Hubbard and Glasser 2005).

Light Detection and Ranging (LiDAR) systems, actively use light, most commonly near infrared, pulsed from a laser to measure distance to the earth's surface (National Oceanic and Atmospheric Administration (NOAA) 2023). LiDAR utilises a shorter wavelength than InSAR and is subsequently affected by cloud cover and rain, but generally has a higher spatial resolution owing to its lower ccost and weight contributing to its suitability as an airborne system (Satsence 2021). Despite their differences, both can be used to produce satellite DEM products with The Shuttle Radar Topography Mission (SRTM) and Advanced Spaceborne Thermal Emission and Reflection Radiometer (ASTER) Global DEM (GDEM), being some of the most popular, both with a 30m spatial resolution (Table 2) (Earth Resources Observation and Science (EROS) Centre 2018; Ghannadi et al. 2023). However, the application of these products for glaciology is limited by their coverage, with SRTM unavailable at extreme latitudes, and ASTER GDEM containing significant holes in both polar regions (Copernicus 2017; Ghannadi et al. 2023). The TerraSAR-X and TanDEM-X twin satellites DEM products are regarded as some of the most accurate and consistent to date (Ghannadi et al. 2023; European Commission 2023). The TanDEM-X DEM is the original non-edited product, other products include WorldDEM and Copernicus DEM (Cop-DEM), the most recent global DEM product, which is available in a range of spatial resolutions, the 30m version of which is popular thanks to its high vertical accuracy (Marešová et al. 2021).

Ghannadi et al. (2023) compared the vertical accuracy of Cop-30m DEM and SRTM using high spatial resolution DEM products and found Cop-DEM to be more accurate than SRTM for both study sites, with a root mean square error (RMSE) of 5.72 and 2.19 meters, compared to 6.10 and 3.95 for SRTM respectively (Ghannadi et al. 2023).

Table 2. Various InSAR and LiDAR satellite-based DEM products (Copernicus 2017; EROS Centre 2018; Marešová et al. 2021).

Satellite	Product	System	Spatial Resolution	Latitudinal coverage
Shuttle Radar Topography Mission (SRTM)	Global Satellite DEM	InSAR	30m	56° S - 60° N
Terra	ASTER GDEM	LiDAR	30m	90° S – 90° N
TerraSAR-X and TanDEM-X	TanDEM-X DEM	InSAR	30m (12m at the equator)	90° S – 90° N
	World DEM	InSAR		90° S – 90° N
	COP DEM	InSAR		90° S – 90° N

An advantage of satellite imagery is their large IFOV, but as a result they lack spatial resolution, additionally satellite DEM products produce huge amount of data that requires filtering and processing, dependent upon its application (Liu 2008). Therefore, pre-processed datasets may not be suitable and consequently, raw data is preferred. However, processing is labour intensive, and methods vary depending on the application, analysis, and data analyst, who may introduce bias (NASA 2023).

1.2.3 Indirect: Passive Imagery and Photogrammetry

Satellite imagery and aerial photographs can be used to measure elevation using photogrammetry, whereby information is extracted about an environment from photographs (Autodesk 2023). The following table introduces the 3 primary principles of photogrammetry.

Table 3. Primary principles of photogrammetry (Zachariah 2019).

Principle	Description
Non-contact measurement	Measurements obtained from a distance, or indirectly.
Collinearity	A correlation between variables; in geometry and photogrammetry, expressed linearly as a set of points along a single line (Dembowski 1968; Liu 2016).
Triangulation	Using known points to determine the location of an unknown point.

Table 4. The paradigms and development of modern photogrammetry.

Paradigm	Description
Analog Photogrammetry 1920s – 1970	Analog photogrammetry began when stereoscopy became widely used, and aeroplanes could be used for aerial imagery (Zachariah 2019).
Analytical Photogrammetry 1960 – 1990s	Used mathematical formulas to calculate the coordinates of a point from photographs using camera calibration parameters, measured image coordinates and ground control points (Ruzgiene and Alekniene 2012; Zachariah 2019).
Digital Photogrammetry 1990s - Present	Further technological advancements and the availability of low-cost computers and cameras helped improve photogrammetry's applications and accuracy (Zachariah 2019; Niculiță et al. 2020).
Laser Scanning 1990s - Present	Development of active airborne and satellite-based systems such as InSAR and LiDAR.

Photogrammetry has been since the advent of photography, as shown in Table 4, and has led to the development of photogrammetric software able to produce a range of outputs shown in Table 5. The process of producing DEMs consists of four key steps. Firstly, photographic alignment, and building a sparse point cloud, followed by building a dense point cloud, then building the mesh, and finally texture (Figure 5) (Swedish National Heritage Board 2019). Some software now allows users to produce DEMs from dense point clouds further reducing processing time.

Table 5. Different outputs produced by photogrammetric software (GeoNadir 2022).

Output	Description
Orthomosaic	A mosaic of images stitched together in photogrammetry software to create a single image
Digital elevation model (DEM)	Multiple types of DEMs including digital surface models (DSM) and digital terrain models (DTM). DSM includes natural and artificial features such as trees and buildings, whereas DTM only models' topography.
3D model/mesh	Computer algorithms can produce 3D models from photos taken from multiple angles to generate a mesh.
Point cloud	Characterised by a collection of points, or coordinates (x, y, z), identified by the software. Photogrammetry software can create both sparse and dense point clouds which are then used to create models.

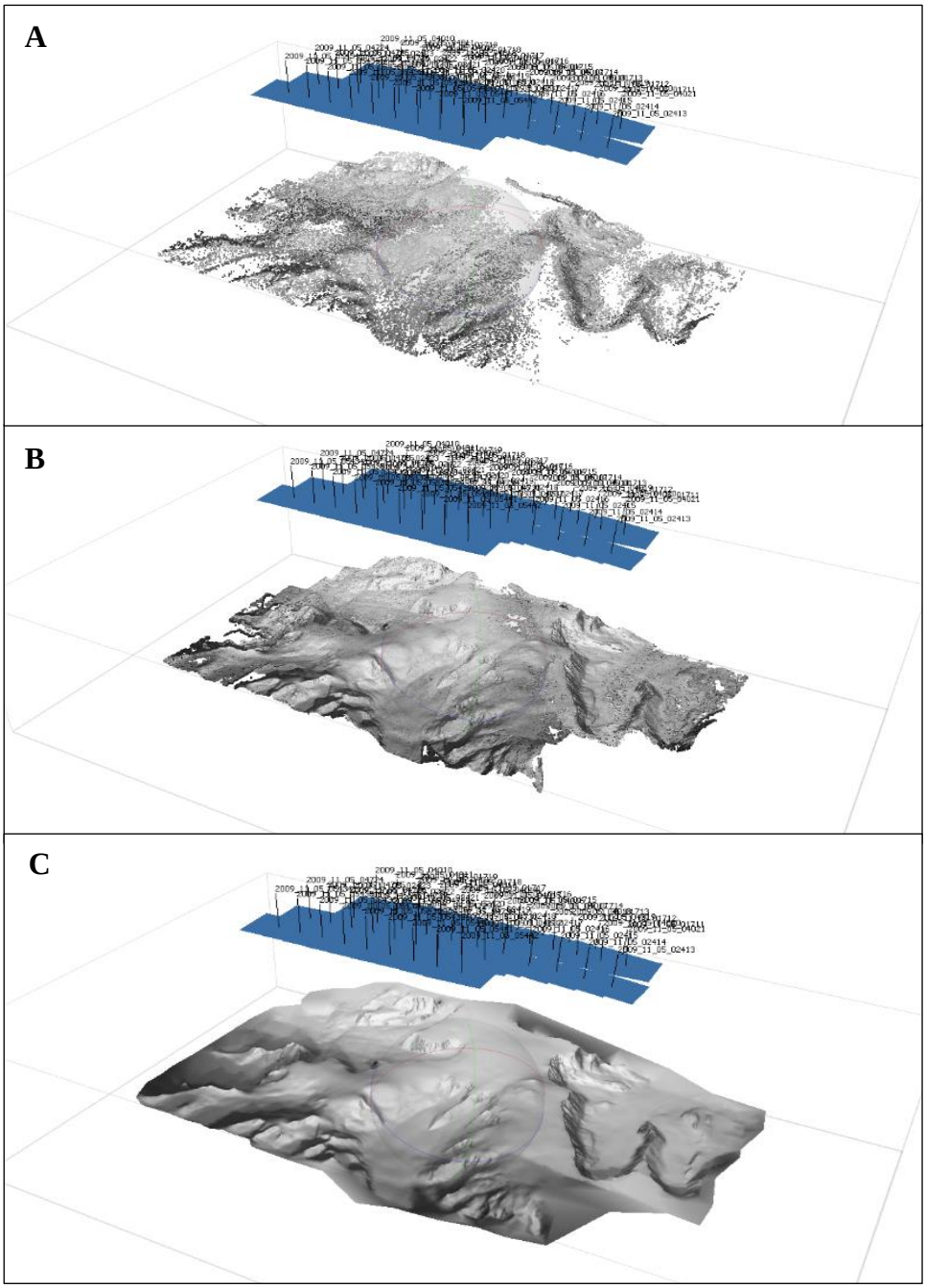

Figure 5. Antartic Peninsula Glacier reconstructed in photogrammetric softwear from Aerial photographs. (A) Sparse Point Cloud, (B) Dense Point Cloud, (C) Mesh.

Aerial photography remains the highest spatial resolution data available for glacial monitoring, owing to its smaller IFOV (Hubbard and Glasser 2005). However, VanLooy et al. (2006) concludes, DEMs are only as accurate as their source data and subsequently their accuracy and precision vary greatly. Fox and Czifersky (2008) discuss how modern photogrammetric techniques can be used to analyse historic aerial photography and reduce

inconsistencies resulting from angle and lens distortion. Their work highlights the difficulties in applying the established Self-calibrating bundle adjustment (SCBA) technique and propose a distortion curve to account for lens distortion (Fox and Czifersky 2008). However, many software packages can now automatically calculate distortion, and subsequently accurate orientation can be achieved even when distortion in unknown.

When using photogrammetry to produce a DEM from aerial photographs, ground control points (GCP) are necessary to provide geographic reference data (Papworth 2014). When using archived photography GCPs are collected after the photos are taken and should be well distributed to ensure the greatest accuracy as discussed in section 3.3 and 5.4. Pulighe and Fava (2013) analysed the accuracy of DEMs created from aerial photographs by comparing them with standard DEM products such as ASTER GDEM and the 10m Italian DEM, TINTIALY (Tintaly 2023). Their assessment was based on known points and confirmed the overall accuracy of photogrammetric DEMs produced from historic aerial photographs as being competitive of those produced by satellite products (Pulighe and Fava 2013).

1.2.4 Summary of Methods

The growing interest in glaciology, coupled with the push for global glacial monitoring in recent years, has led to the rapid development of indirect, remote sensing methods for measuring elevation (Davies 2020a; Li et al. 2021). However, indirect methods lack spatial resolution and subsequently direct, measurements are often necessary to support and improve the overall accuracy of calculations (Cox and March 2004; Li et al. 2021). As stated by Fischer (2011), both direct and indirect mass balance methods are valuable and largely complement each other. As a result, many studies prefer to use multiple measures of mass balance. Zemp et al. (2019), produced a global glacier mass change dataset composed of both glaciological and geodetic measurements collected by the World Glacier Monitoring Service (WGMS) from 1961-2016 (Li et al. 2021). Long-term global datasets such as these, enable scientists to identify trends in mass balance (Kurtz 2013). Li et al. (2021) define 20 years as the minimum period for which long-term trends may be assessed when monitoring glacial changes. Therefore, when measuring multi-decadal changes in elevation photogrammetry is utilised due to the lack of historic In-SAR and Lidar datasets.

Table 6. Summary of methods used to measure Glacier elevation discussed in section 1.2.

Method	Strengths	Weaknesses	Accuracy	Precision
Staking	High spatial and temporal resolution. Simple and inexpensive.	Interpolated from seasonal measures. Time consuming and labour intensive.	Medium	Medium
GNSS Survey	High spatial and temporal resolution. User has control over point frequency.	Interpolated from seasonal measures. Very expensive, time consuming and labour intensive. High volume of data, a lot of processing.	High	High
In-SAR	Active system utilising long wavelengths. Can be used to measure bed topography.	High volume of data, a lot of processing. Low-medium spatial resolution.	Medium	Medium
LiDAR	Active system utilising short-medium wavelengths. Airborne or spaceborne systems.	High volume of data, a lot of processing. Affected by cloud cover and rain.	Medium – High	Medium
Passive Imagery and Photogrammetry	High spatial resolution. Historic photographs available. Various outputs.	Requires GCPs and georeferencing.	Medium - High	Medium - High

1.3 Study Area: Antarctica.

Growing concerns regarding climate change has seen the number of published articles on glacial mass balance increase dramatically (Figure 6). Antarctica is of special scientific interest as the largest and most pristine environment on earth, with collections of aerial photographs dating back to the 1940s. Whilst ice sheets hold the majority of Earths freshwater, glaciers currently account for 60% of the ice mass lost in Antarctica with contributions from smaller glaciers predicted to cause 0.1-0.25m of additional sea-level rise by 2100 (Meier et al. 2007). As stated by Dong et al. (2021), the Antarctic Peninsula has been widely studied due to its sensitivity to climate change and potential contribution to global sea level. Additionally, there is growing interest in the spatial variation of mass loss on the Antarctic Peninsula with the Western Peninsula warming fastest and Eastern Peninsula retreating fastest (Turner et al. 2020; Cook 2014).

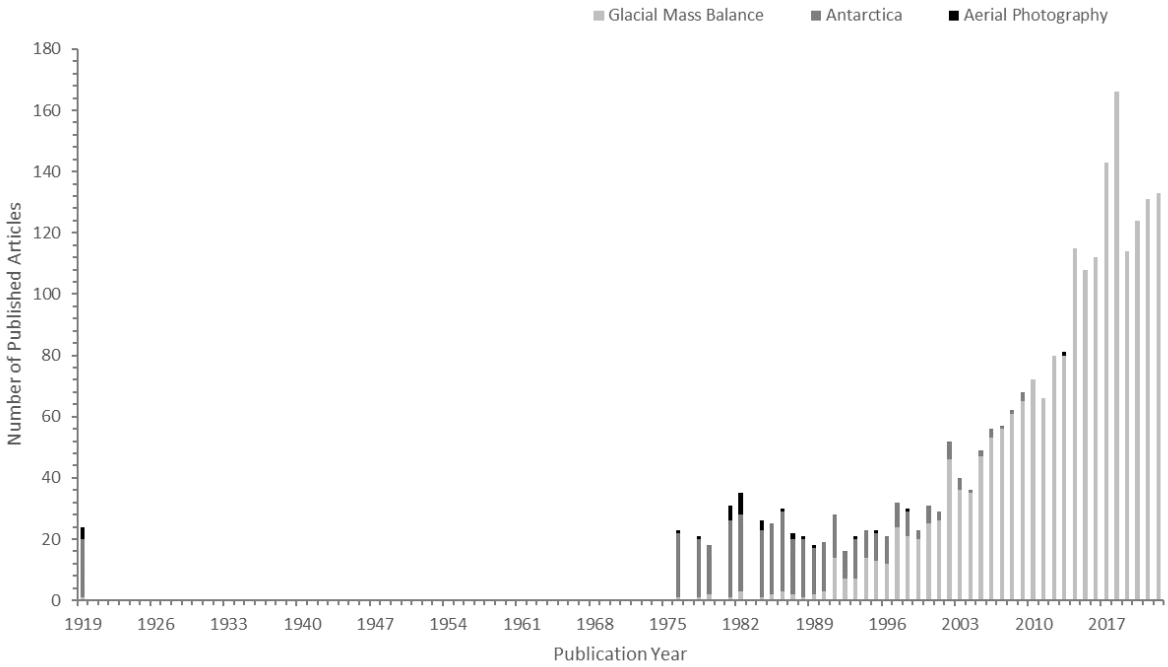

Figure 6. Stacked bar chart displaying the number of published articles identified by Clarivate Web of Science (11th of November 2022) and associated publication years. Glacial mass balance results identified from search topics, “glacial mass balance”. Antarctica results from search topics, “glacial mass balance” and abstract “Antarctic” OR Antarctica”. Aerial Photography results identified from search topics, “glacial mass balance” and abstract “Aerial photography” OR Photogrammetry”.

Data collected from NASAs Gravity Recovery and Climate Experiment (GRACE) and GRACE follow up (GRACE-FO) satellites, Figure 7, further highlights the accelerating rate at which mass is being lost in Antarctic. NASAs GRACE and GRACE-FO satellites study changes in water, ice sheet and the solid earth using a microwave k-band ranging instrument, accelerometer, and GNSS receiver to detect changes in the pull of gravity (Gricius and Hartono 2023). The GRACE satellites are the first to map gravitational changes on earth, which is an alternative way of measuring mass balance, and is particularly useful when estimating the mass of large ice sheets (Leroux and Pellarin 2016). However, with a spatial resolution of approximately 300km, GRACE lacks the spatial resolution necessary for investigating glaciers at fine scales and thus high-resolution methods are required (Dong et al. 2021).

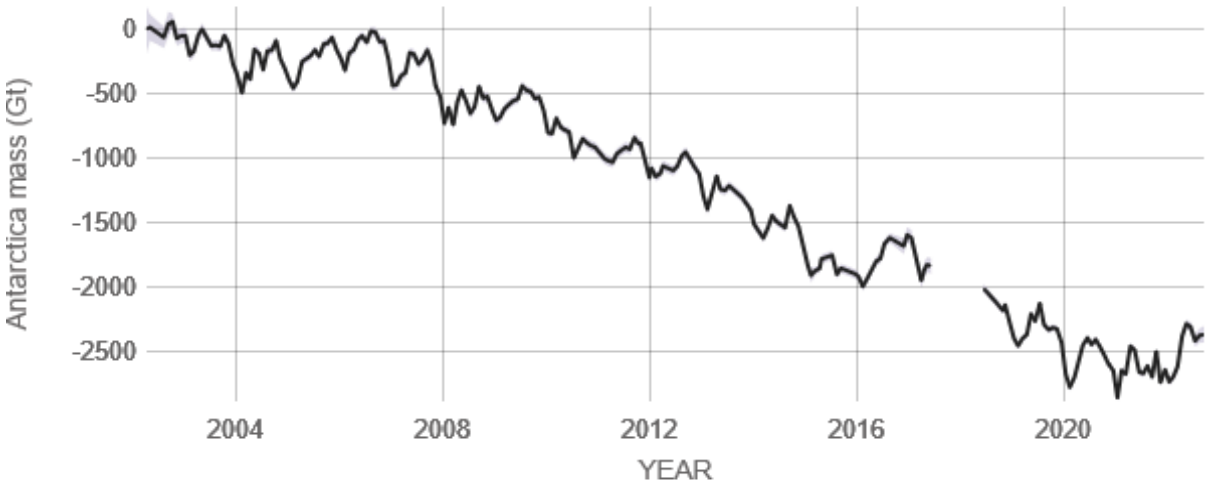

Figure 7. Change in volume (Gt) of Antarctic Terrestrial Ice Mass from 2002-2022, measured by NASAs GRACE and GRACE-FO satellites, obtained from NASA (2022). Missing data from June 2017 until June 2018 due to the time between GRACE and GRACE-FO satellite missions (NASA 2022).

The thinning and retreat of marine terminating glaciers is associated with dynamic instability, which Meier et al. (2007) highlights, is generally not considered in mass-balance and climate modelling. By comparing retreat rates on the Antarctic Peninsula to the climate record, Pudelko et al. (2018) found interannual fluctuations to be correlated to oscillations in annual Positive Degree-Days. Suggesting that whilst mass loss on the Peninsula is somewhat continuous, interglacially there is still huge variation in response (Pudelko et al. 2018). Furthermore, morphology plays a key role in frontal recession and glacial thickness. Pastik et al. (2021) observed longitudinal slope on marine terminating glacier to be the connecting factor between front position and glacier thickness, with steeper slopes resulting in thinning

and retreat. Previous studies have investigated difference in behaviour associated with terminus, with marine-terminating glaciers most vulnerable to climate change (Davies et al. 2012). Additionally, the role of aspect on glaciation has been observed to be of local significance at mid-latitudes but is not obvious regionally (Benn and Evans 1998; Huber et al. 2017; Geçen et al. 2018). Despite this, little work has been done to better the role of aspect on mass balance at extreme latitudes. Thus, by comparing two glaciers with opposing aspects, on the east and west coasts of the Antarctic Peninsula, this report will investigate to what extent aspect, effects multi-decadal changes in glacial thickness.

2.0 Aim and Objectives

2.1 Aim

To assess the influence of aspect on marine terminating glaciers on the East and West coasts of the Antarctic Peninsula and compare decadal changes in elevation as a measure of glacial mass balance.

2.2 Objectives

Objective 1 – Identify appropriate marine terminating glaciers with opposing aspects and similar characteristics located at extreme latitudes.

Objective 2 – Identify high-resolution aerial photographs of Antarctic Peninsula Glaciers, Leonardo and Diplock, to measure multi-decadal changes in glacial thickness.

Objective 3 – Create digital elevation models using available computer software's using high-resolution aerial photography.

Objective 4 – Compare and contrast changes in elevation of both glaciers and discuss their similarities and differences, in addition to changes in their size and shape.

Objective 5 – Discuss to what extent aspect contributes to observed changes in elevation of both glaciers, using supporting evidence from previous studies and elevation profiles.

3.0 Methods

Multi-decadal changes in elevation were measured for two marine terminating glaciers of opposing aspect and similar characteristics on the Antarctic Peninsula. Archived film and more recent digital aerial photographs were used to build DEMs and assess the change in elevation, size, and shape of chosen glaciers.

3.1 Study Area

Two glaciers were identified from the World Glacier Inventory (Figure 8). Diplock on the east coast of the Antarctic Peninsula and Leonardo on the west coast. The glaciers were selected based on available archived aerial photographs, aspect, and terminus. Diplock and Leonardo, are both marine-terminating and partly sheltered by offshore land masses shown in Figure 8. However, they are situated at different latitudes, and have slightly varying characteristics resulting from the topography of the Peninsula.

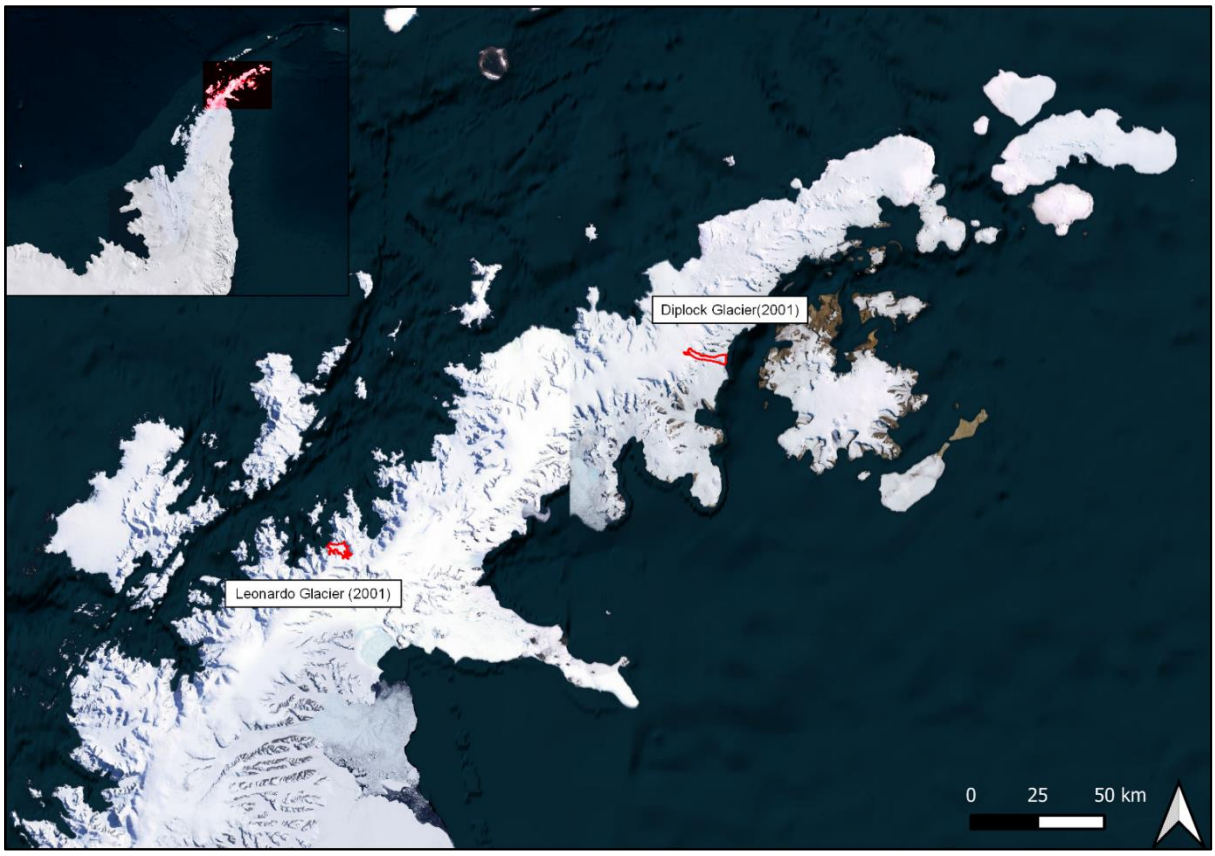

Figure 8. Antarctic Peninsula Glaciers, Leonardo and Diplock, polygonised extents as of 2001 based on Aster Imagery (Rau et al. 2005), shown in red, overlaying Bing Virtual Earth Base Map with wider extent shown in the top right.

Leonardo glacier is a westward facing (270°) marine-terminating outlet glacier, located -64.69870'N and -61.88970'W, with a total area extent of approximately 25km^2. In addition, Leonardo has a cascading or stepped longitudinal profile which may inhibit flow and allude to the stationary classification of its tongue (Rau et al. 2005).

Table 7. Characteristics of Leonardo Glacier as classified by Global Land Ice Measurements from Space (GLIMS) classification system manual V.1 by Rau et al. (2005), based on 2001 ASTER imagery.

Characteristic	Classification	Description
Primary Classification	Outlet Glacier	Flows downslope, following local topography with no clearly defined catchment.
Form	Compound Basins	System of valley glaciers that merge into one basin.
Longitudinal Profile	Cascading	Surface varies in inclination, crevasses and seracs common.
Source Nourishment	Snow / Drift Snow	Snow and wind transported accumulation.
Activity of Tongue	Stationary	Not moving.
Frontal Characteristics	Floating	Terminus is floating, implies calving.

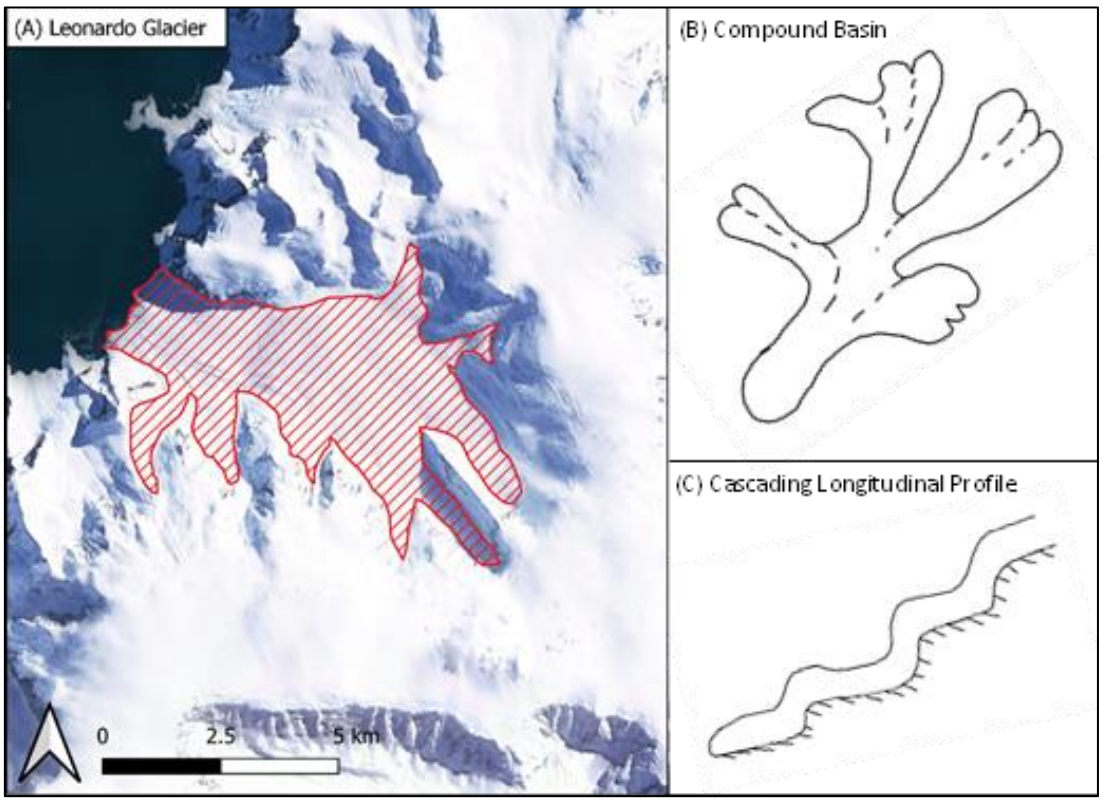

Figure 9. (A) Leonardo approximate glacial extent. (B) Diagram of Compound Basin Glacier form, and (C) Diagram of Cascading Longitudinal Profile inspired by Rau et al. (2005).

Diplock is an eastward facing (90°) marine-terminating confluent outlet glacier, located -64.02642'N and -58.90817'W, with a total area extent of approximately 33km^2. Diplock merges masses with a glacier of similar size along the northern edge of its tongue approximately 3km from its terminus (2001) (Jiskoot 2014) (Figure 10). Furthermore, due to lack of data, Diplock's tongue activity has not been classified (Table 8) (Rau et al. 2005).

Table 8. Characteristics of Diplock Glacier as classified by GLIMS classification system manual V.1 by Rau et al. (2005), based on 2001 ASTER imagery.

Characteristic	Classification	Description
Primary Classification	Outlet Glacier	Flows downslope, following local topography.
Form	Simple Basin	Single basin with catchment defined by topography.
Longitudinal Profile	Even, regular	Regular stepped longitudinal profile with little variance in surface.
Source Nourishment	Snow / Drift Snow	Snow and wind transported accumulation.
Activity of Tongue	Uncertain	Uncertain, or not measured.
Frontal Characteristics	Confluent	Tongue merges with another glacier.

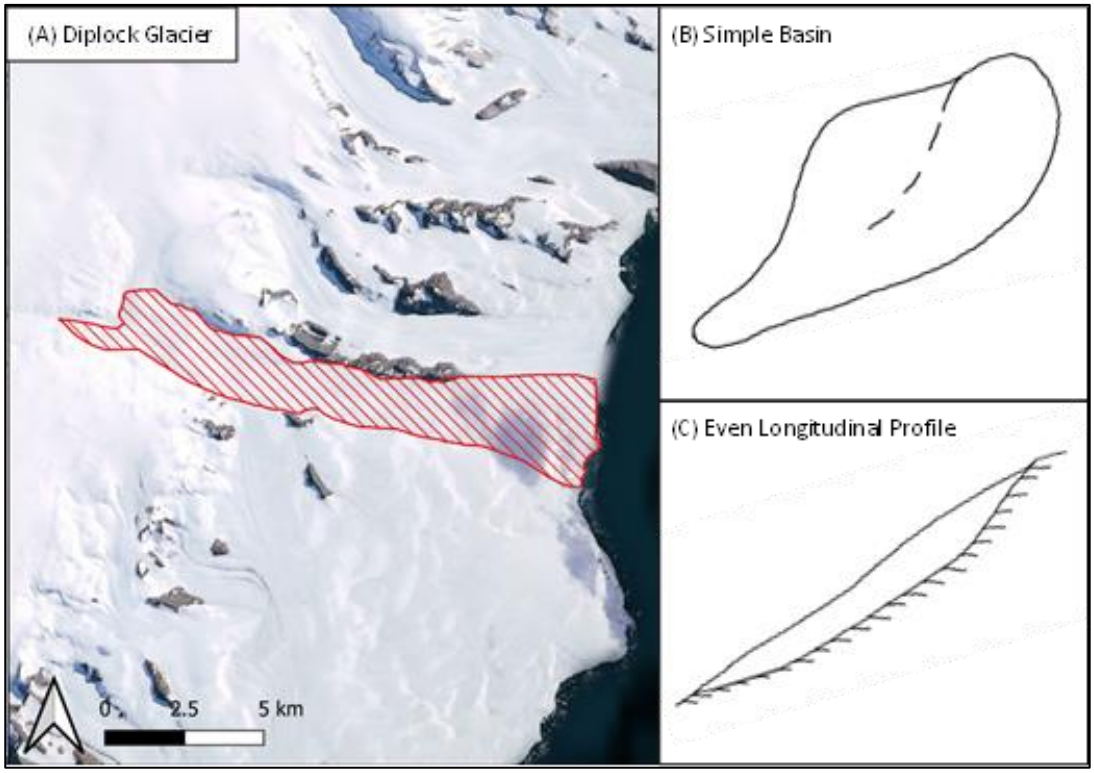

Figure 10. (A) Diplock approximate glacier area. (B) Diagram of Single Basin Glacier form and, (C) Diagram of Even, regular, Longitudinal Profile inspired by Rau et al. (2005).

3.2 Aerial Photography

High-resolution digitised archived film photographs were obtained from the British Antarctic Survey (BAS) (1956-1957). The photographs were taken using three Fairchild cameras with 6-inch Bausch and Lomb 90-degree metrogon lenses stored on 9-inch film (National Air and Space Museum 2023). The cameras were calibrated by the National Bureau of Standards for use for aerial photography and assembled with one vertical axis, and two oblique axis (Figure 11) (Global Security 2023; National Air and Space Museum 2023). For this project only overlapping vertical photographs were used in produce DEMs. Camera calibrations outlined in Table 9, were provided by BAS Mapping and Geographic Information Centre upon request.

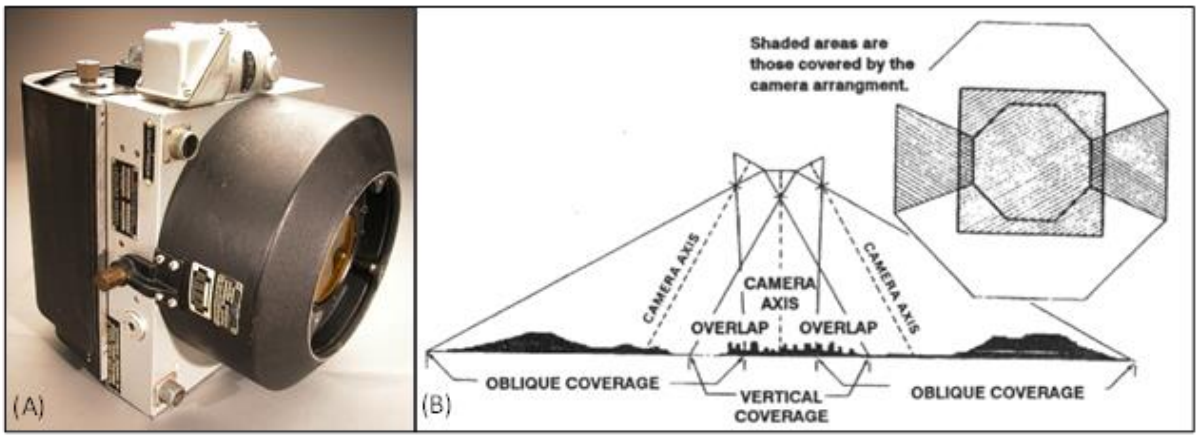

Figure 11. (A) Fairchild camera (National Air and Space Museum 2023). (B) The camera axis and overlap of trimetrogon aerial photography (Global Security 2023).

Operation Icebridge was flown between 2009-2016, to bridge the gap between the Ice Cloud and land Elevation Satellite (ICESat) missions. Icebridge used a fleet of aircraft equipped Digital Mapping Systems (DMS), which acquired high spatial resolution natural colour (RGB) and panchromatic imagery (Dominguez 2019). Most photographs were obtained in panchromatic mode to maximise grey-level possibility, but all outputs are natural colour (RGB) (Dominguez 2019). The DMS system included a 21-megapixel Canon EOS 5D Mark II digital camera, computer-controlled intervalometer to ensure the correct spacing between frames, and an Applanix POS/AV precision orientation system (Dominguez 2019; Anagnostopoulos 2023). Images were also adjusted in-flight to increase quality and exposure (Dominguez 2019).

Table 9. Collections of aerial photographs identified for Leonardo and Diplock.

Leonardo				
Dataset	Year	Focal Length	Flying Height	Resolution (dpi)
BAS 26/FID	1957	153.21 mm	13500 ft	96
IceBridge DMS L0	2009	28.00 mm	Low - Medium	72
Diplock				
Dataset	Year	Focal Length	Flying Height	Resolution (dpi)
BAS 26/FID	1957	153.21 mm	13500 ft	96
IceBridge DMS L0	2016	28.00 mm	Low - Medium	72

3.3 Pre-processing

The Icebridge Level-0 raw imagery was downloaded in JPEG format, whilst BAS film photographs were converted from GeoTIFFs to JPEGs, with a compression value of 75%. Additional pre-processing was required for the film photographs including resizing using photo editing software, and masking film frames and frame numbers in photogrammetric software to avoid misalignment. Fiducials were also present on each image, but their coordinates are unknown and as a result, were excluded.

GCPs were used to provide geographic references for both the film and digital photography (Papworth 2014). Nunataks were identified as the most suitable GCPs, and their position was obtained from existing DEM products. NASAs Icebridge airborne Lidar had the highest spatial resolution but had limited coverage for both glaciers. As a result, GCPs were not well distributed and caused issues with scaling in photogrammetry software. Therefore, Cop-30m DEM was used due to its high vertical-resolution as discussed in section 1.2.2. According to Copernicus (2017), Cop-DEM has a vertical resolution of 1m and accuracy of 7m, which is in alignment with the accuracy observed by Ghannadi et al. (2023). Additionally, Cop-DEM uses the horizontal reference datum World Geodetic System 1984 (WGS84 EPSG 4326) the same as the LIMA mosaic created from Landsat 7 imagery, with a 30m resolution, which was also used when identifying GCPs (Ghannadi et al. 2023). The distribution of GCPs for both Leonardo and Diplock is shown in figure 12, with a minimum of 60 GCPs per DEM to ensure sufficient geographic reference (Papworth 2014).

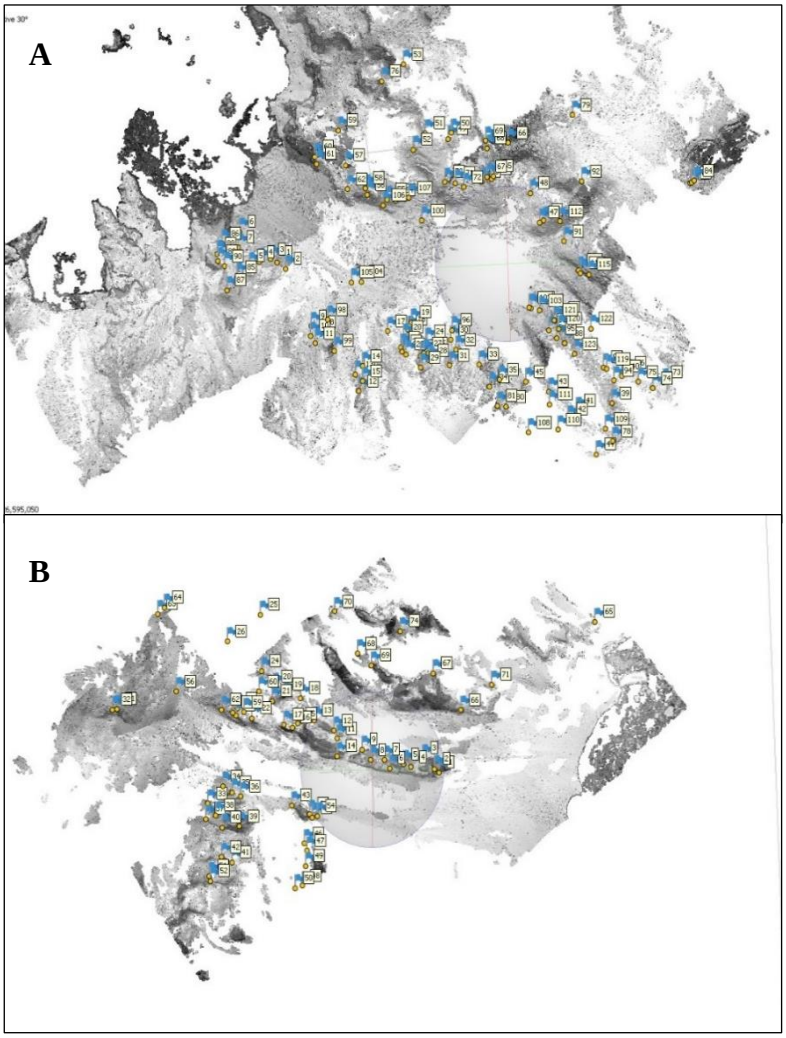

Figure 12. Distribution Ground Control Points for (A) Leonardo, and (B) Diplock, overlying dense point cloud in photogrammetric software.

3.4 Photogrammetric Analysis

Following pre-processing the photogrammetric software, Agisoft Metashape Professional, was used to build DEM following the process outlined in Figure 13. DEMs were built from depth maps created when building a dense point cloud using aggressive filtering to ensure the greatest accuracy. Figure 14 shows different DEMs built from a mesh, dense point cloud and depth maps to highlight the variation in accuracy associated with each approach. Additionally, interpolation was enabled as default to fill minor holes within the model. Holes are the result of very smooth, untextured surfaces lacking tie points such as on the glacier tongue.

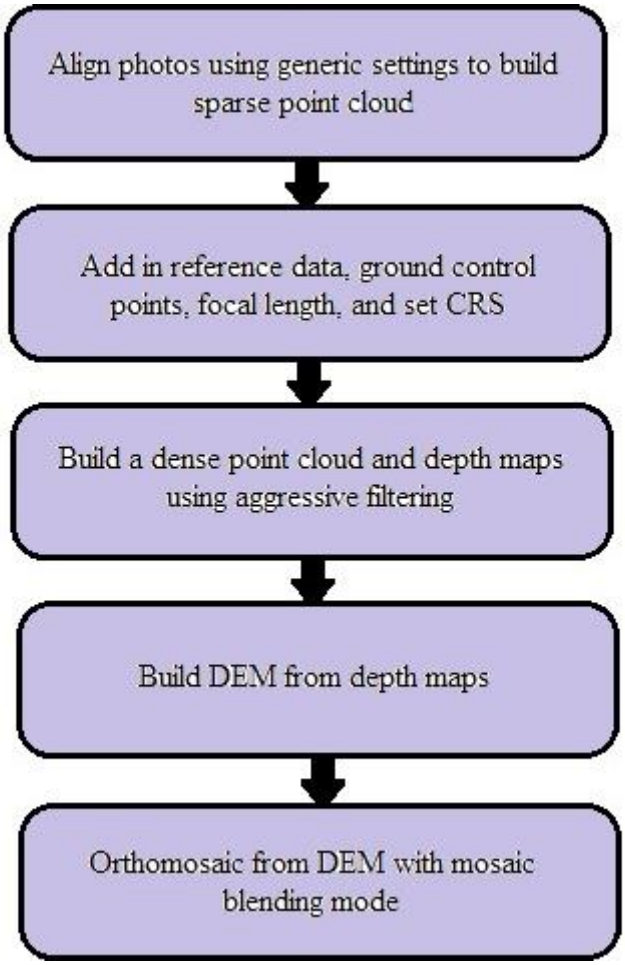

Figure 13. Step by step process of building DEM and Orthomosaic from archived film photography in photogrammetry software.

DEMs created in photogrammetric software were exported as Geotiff files to avoid any compression and imported into Quantum GIS (QGIS) for analysis. During analysis the Raster Calculator was used to subtract the Icebridge DEM from the BAS DEM, based on the assumption that both Leonardo and Diplock had lost mass over the period, to produce a delta, or difference DEM. In addition, an orthomoasic was created from each set of photographs to produce a high spatial resolution image from which glacier extent could be measured. Orthomosaics were also exported as Geotiffs and imported into QGIS for analysis.

To assess the accuracy of DEMs the United States Geological Survey (USGS) suggest using at least 28 check points to validate GCPs (Papworth 2014). However, as discussed in section 3.3, GCPs are limited to Nunataks and subsequently not evenly distributed. Additionally, GCPs are only as accurate as the product they are derived from and as a result each GCP has an estimated error based on the analyst's confidence in its precision. Photogrammetric software then uses each GCPs estimated error, number of projections and quality of

alignment to generate the predicted of each GCP. The absolute error was used to assess the accuracy and precision of each DEM shown in Table 12, where the absolute error is the modulus of the observed and predicted errors. Root mean square error (RMSE) and mean error (ME) were used as a measures of accuracy, and standard deviation (SD) as a measure of precision discussed in section 5.4 (Papworth 2014).

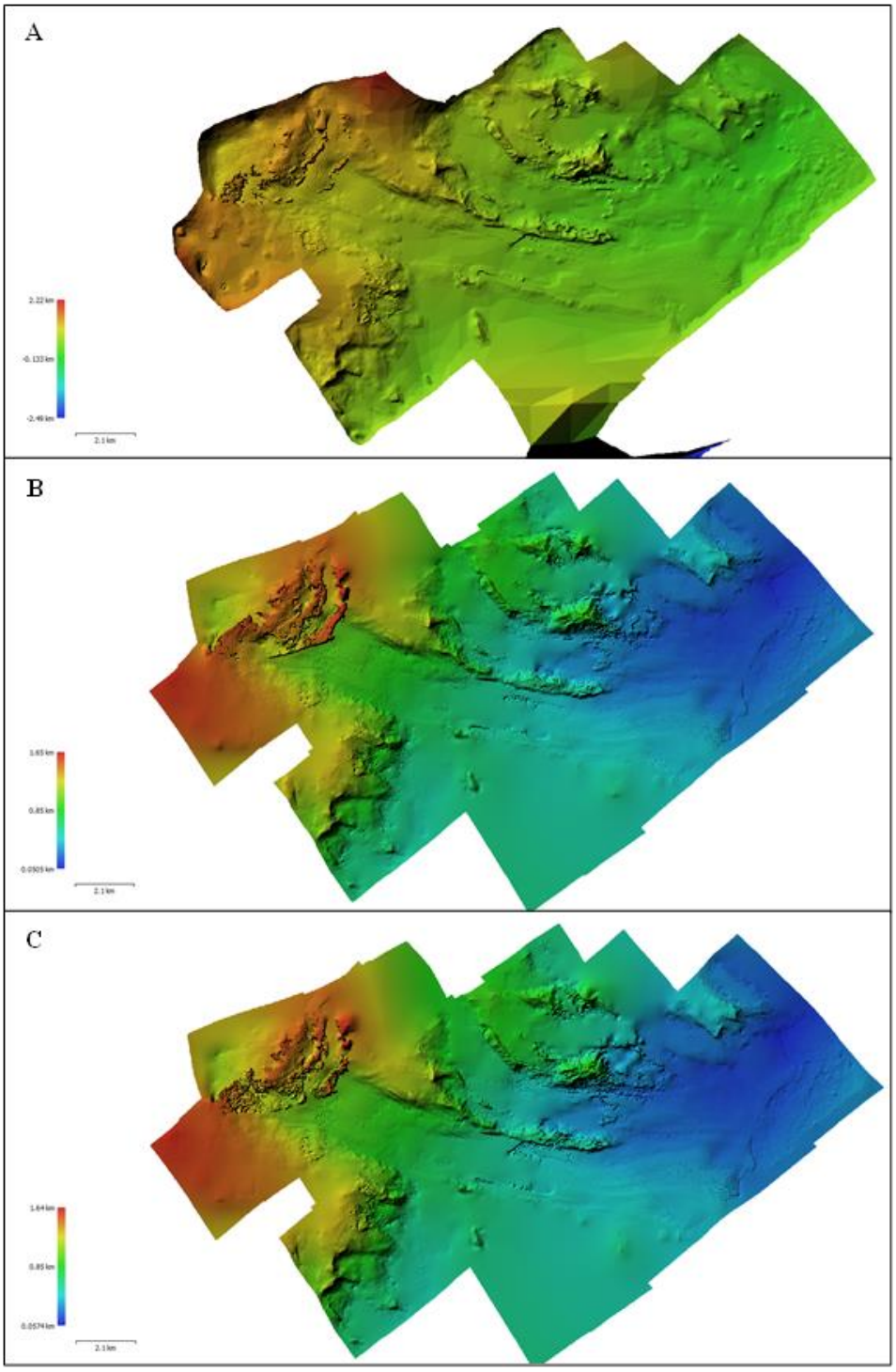

Figure 14. DEMs of Diplock built using film photography. (A) DEM built from mesh using TIN interpolation, (B) DEM built from dense point cloud, (C) DEM built from depth maps.

4.0 Results

In the following section the DEMs produced from both BAS and Icebridge aerial photographs are presented in addition to Table 12 summarising their accuracy and precision. Additional figures have been produced to show area extent and change in shape and size over the period measured. Two key themes were identified in these results, change in glacier thickness, and change in glacier shape, each of which are discussed in the following sections and summarised in Table 13.

4.1 Change in Elevation

The first set of DEMs shows obvious thinning of Leonardo from 1957-2009 at the glacier head, with little change observed along the glacier tongue. Change in elevation at the terminus is unknown due to incomplete coverage and insufficient overlap of aerial photographs discussed in section 5.4. To compare the difference in elevation a delta DEM was built, shown in Figure 16, with 100m contours to highlight the distribution of change across the glacier surface. Changes in elevation and slope are presented as an elevation profile, Figure 17. The most striking result from all three figures is the obvious thinning at the glacier head in contrast to the glacier tongue.

Overall, Leonardo lost 1618.83m of elevation between 1957-2009, equal to a 29.4% of its 1957 elevation. As shown in Figure 17, 616.25m of elevation was lost at the glacier head, along the north-eastern edge, highlighted by contours in Figure 16. However, mass loss decreased with distance from the glacier head, along the centre line, where approximately 3km from the head the glacier surface began to rise, resulting in an increase in elevation of 79.40m, 7.4km from the glacier head. The resulting change in size, shape and slope profile is discussed in section 4.2.

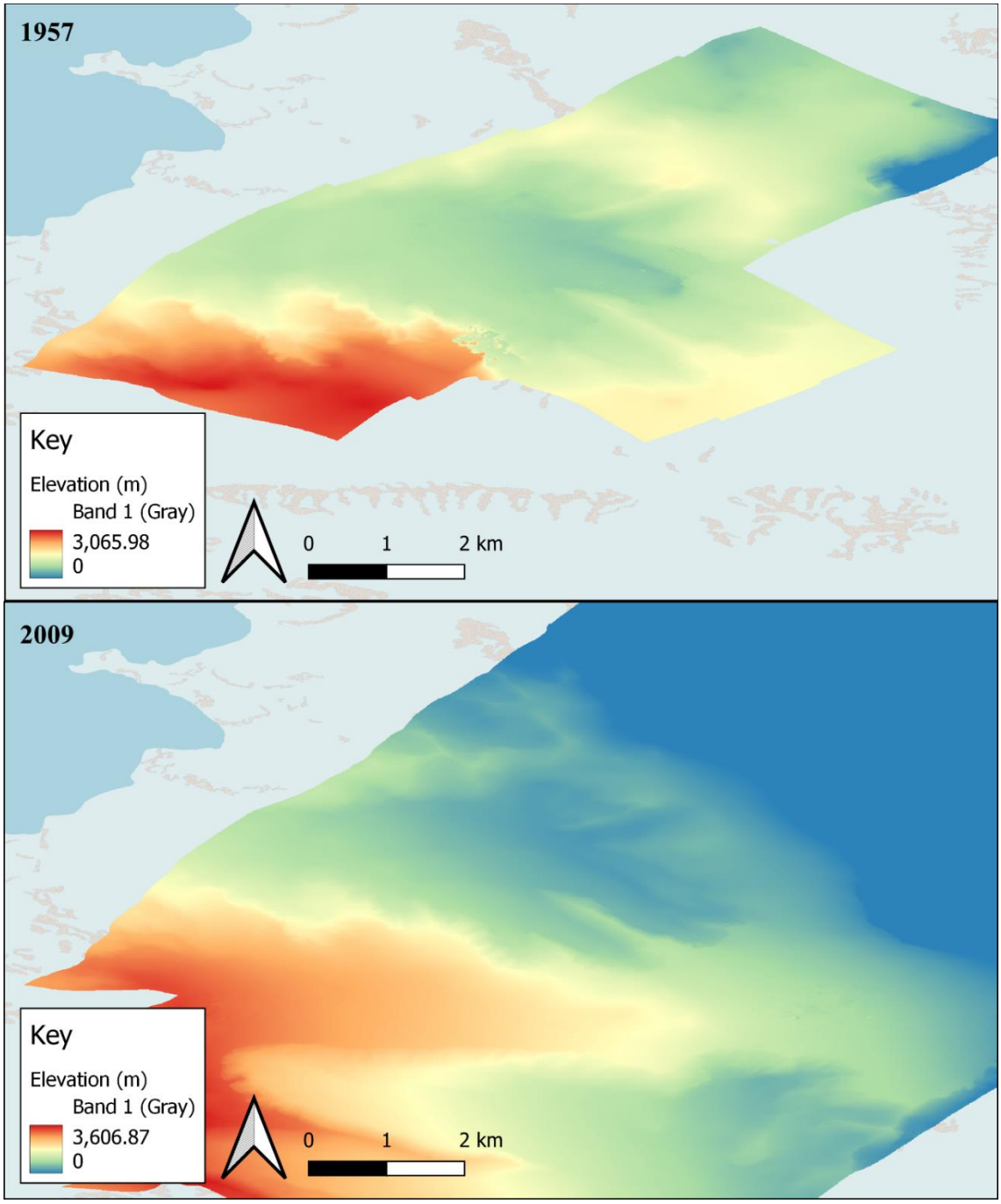

Figure 15. Digital elevation models produced using aerial photographs of Leonardo in 1957, and 2009, overlying OpenSteetMap basemap.

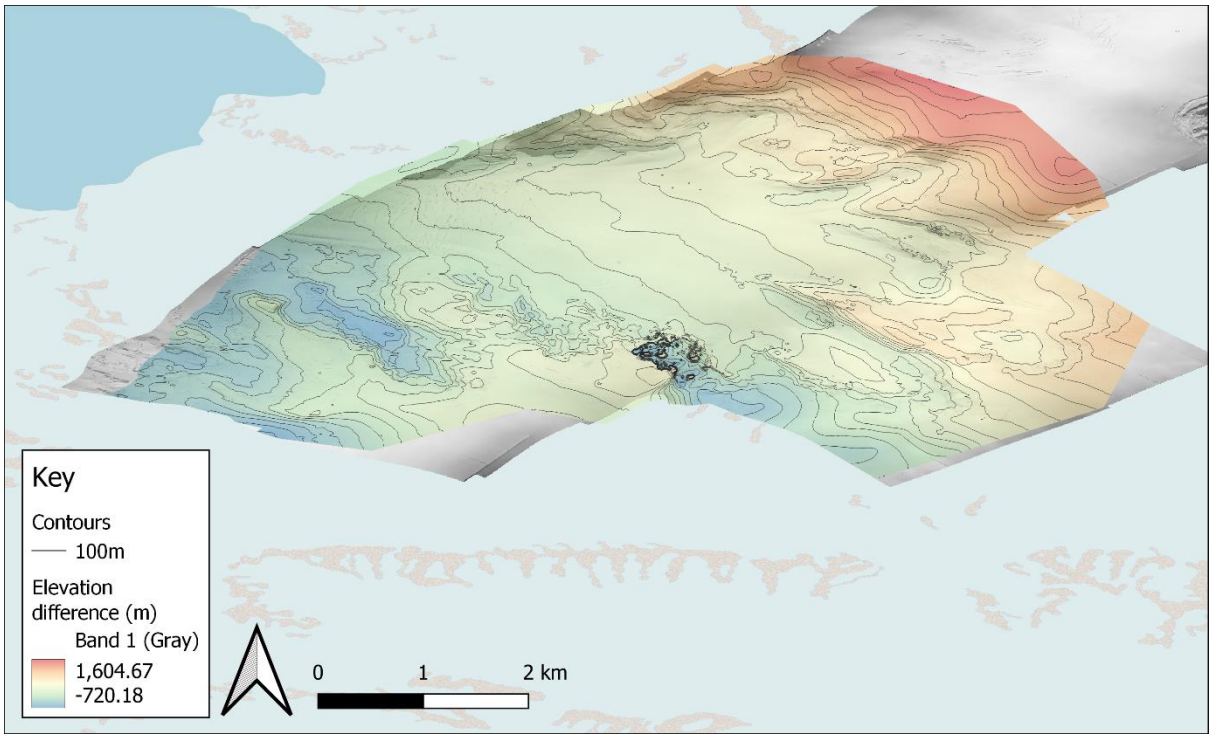

Figure 16. Delta DEM and 100m contours of Leonardo surface showing the difference in elevation from 1957-2009, overlying BAS 1957 orthomosaic and OpenStreetMap basemap.

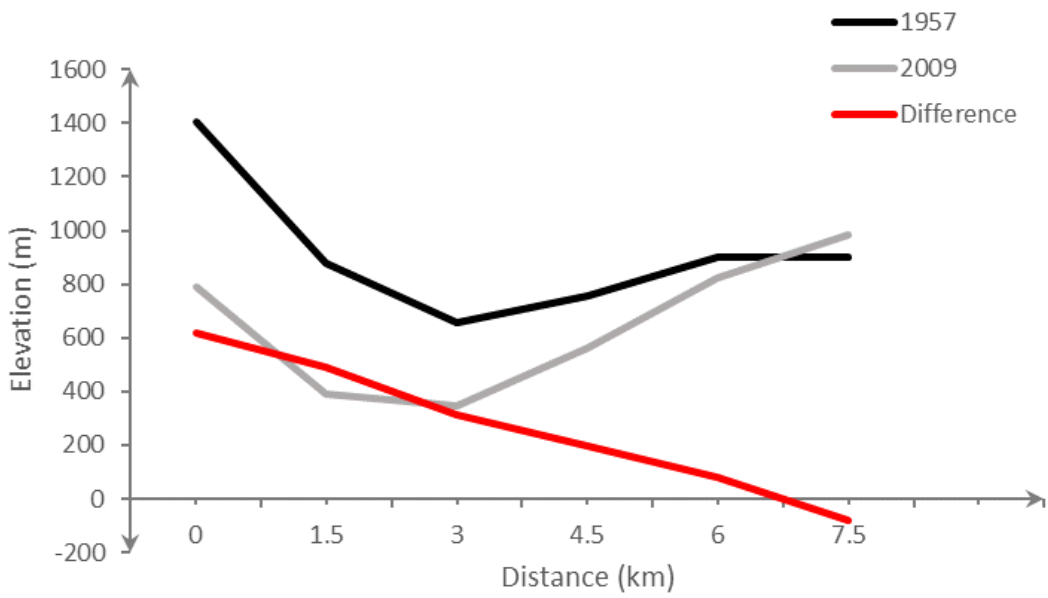

Figure 17. Centre line elevation profile of Leonardo in 1957, 2009 and change in elevation with distance from the head of the glacier. Elevation obtained from DEMs built using aerial photographs in addition to delta DEM.

The change in elevation observed for Diplock between 1957-2016 is presented as two DEMs in Figure 18. The greatest loss is observed at the terminus and a small gain at the glacier head, resulting in an overall steepening of the glacier. However, elevation values at the glacier head from 1957 are slightly misleading due to the presence of clouds. Additionally, incomplete coverage of Icebridge aerial photographs resulted in merged DEM with Cop-30m DEM produced from the TanDEM-X DEM discussed in section 1.2.2 and 5.4 (Copernicus 2017).

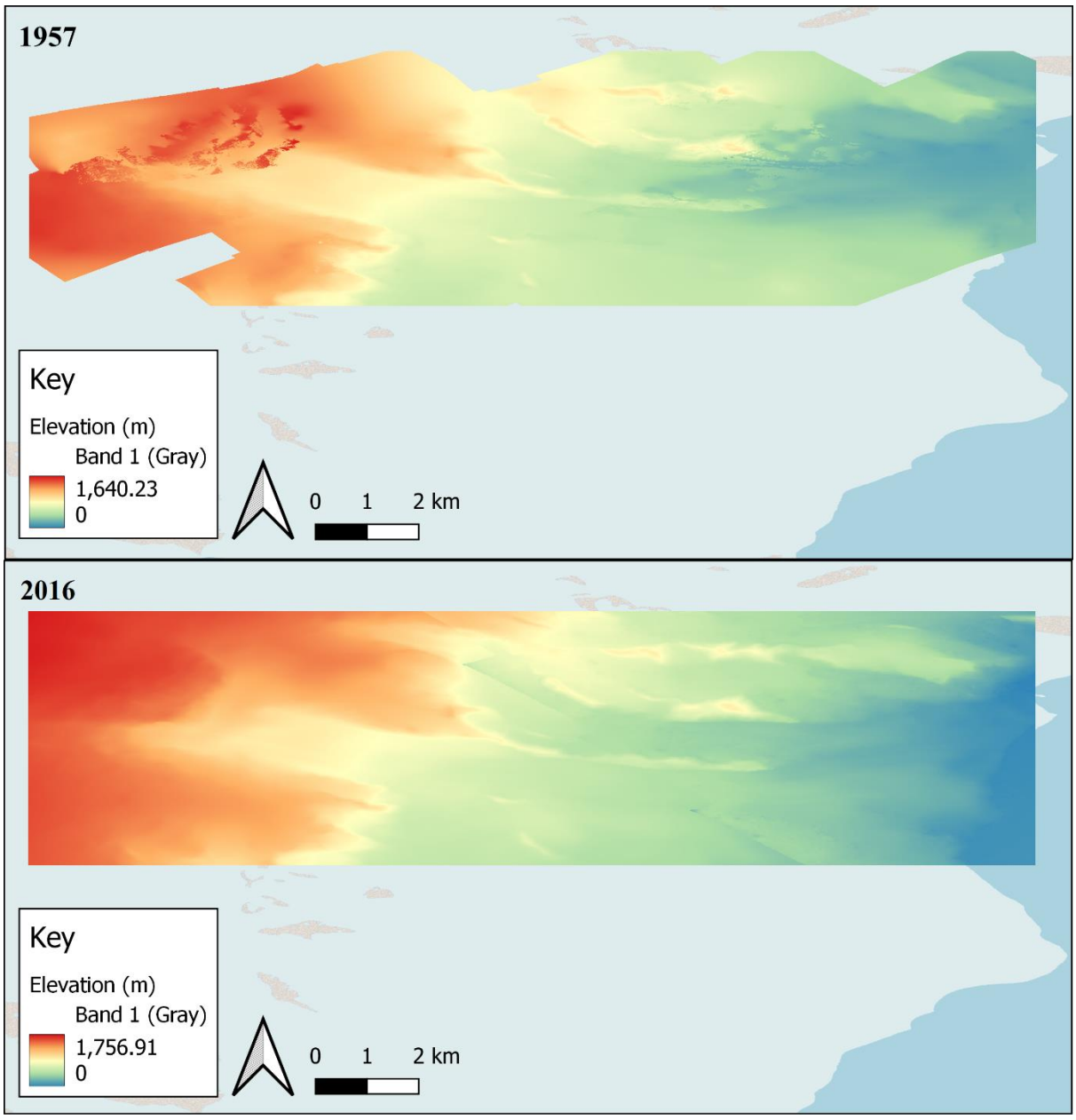

Figure 18. Digital elevation models produced using aerial photographs of Diplock in 1957, and 2016, overlying OpenSteetMap basemap.

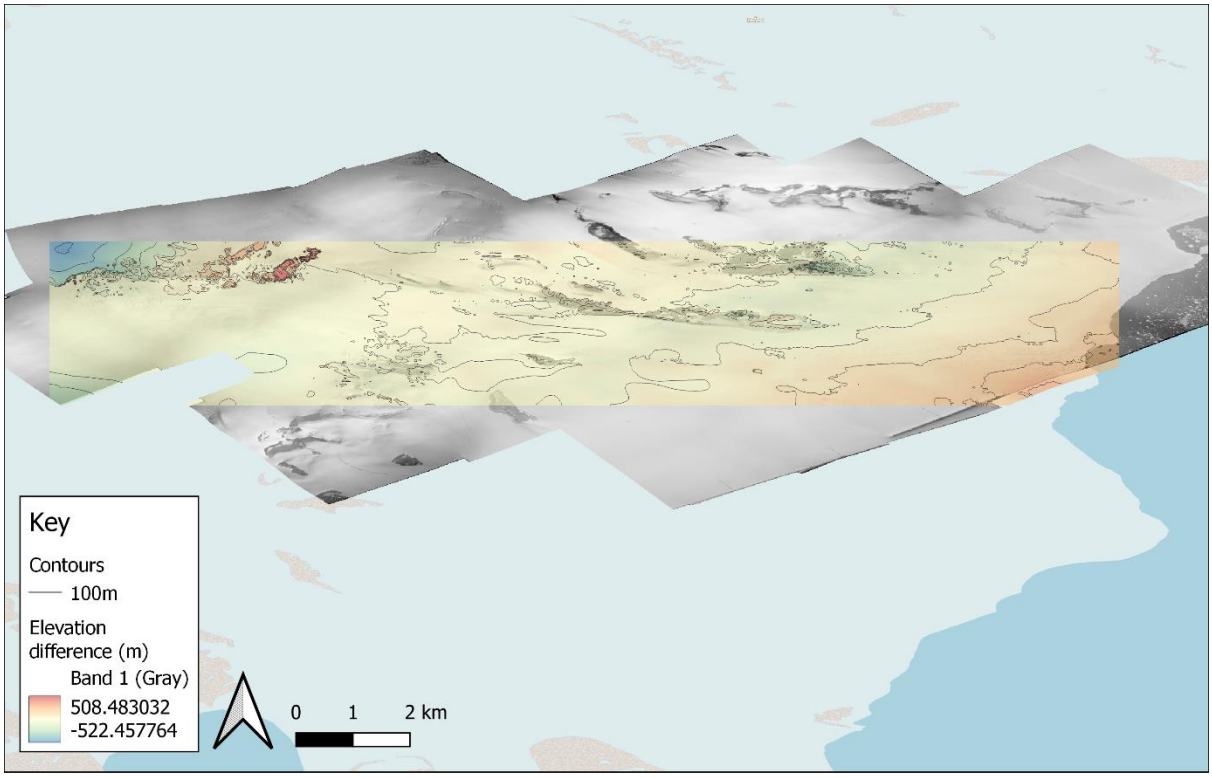

Figure 19. Delta DEM and 100m contours of Diplock surface showing the difference in elevation from 1957-2016, overlying BAS 1957 orthomosaic and OpenStreetMap basemap.

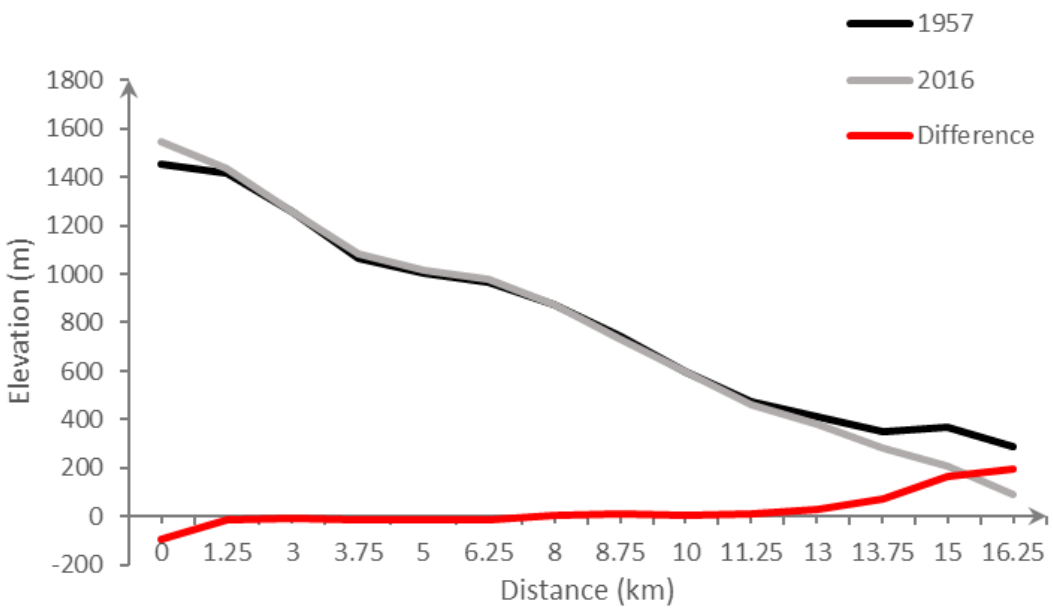

Figure 20. Centre line elevation profile of Diplock in 1957, 2016 and change in elevation with distance from the head of the glacier. Elevation obtained from DEMs built using aerial photographs in addition to delta DEM.

Overall 349.59m of elevation was lost between 1957 and 2016, equivilent to 3.1% of Diplocks 1957 elevation. Figures 19 and 20, show the distribution of elevation change across the glacier surface as elevation increases with distance from the head. Figure 20 shows a 198.97m lost at the terminus and 92.01m gain on the southwestern glacier head. This is highlighted again in Figure 18 and 19, as changes >15m are limited to the glacier head and terminus resulting in a change in shape and slope profile, discussed in the following section.

4.2 Glacier Shape and Size

The observed changes in elevation discussed in section 4.1, resulted in changes in the size, shape, and slope profile of both Leonardo and Diplock. Glacier extent for both Leonardo and Diplock are shown in Figure 21 and 22. Surface area was calculated from polygons created using Orthomosaics created from BAS and Icebridge aerial photographs. Leonardo Icebridge 2009 aerial photographs did not provide full coverage of the glacier and subsequently extent was calculated from 2009 Landsat 7 imagery. Similarly, 2016 Landsat 8/9 imagery was used to extrapolate the extent of Diplock 2016 discussed in section 5.4. Additionally, Leonardo's 1957 BAS Orthomosaics could not be successfully merged within photogrammetric software, due to insufficient overlap, and were instead overlaid to produce a base image for measuring extent.

Over the period measured both glaciers changed in size as outlined in Table 10, with Diplock loosing 10,250.51 m^2 of surface area, at a rate of -174.25 m^2 p.a. (per annum), and Leonardo loosing 2,943.32 m^2 at a rate of -56.60 m^2 p.a.. Additionally, both glaciers experienced thinning, as previously discussed, with Leonardo experiencing the greatest rate of thinning, -31.12 m p.a., and Diplock, -5.93 m p.a. outlines in Table 14.

Table 10. Glacier extent of Leonardo and Diplock outlined in Figure 21 and 22.

	Leonardo	Diplock
1957 extent	27,961.51 m^2	41,989.31 m^2
2009/2016 extent	25,018.19 m^2	31,708.80 m^2
Difference	-2,943.32 m^2	-10,280.51 m^2

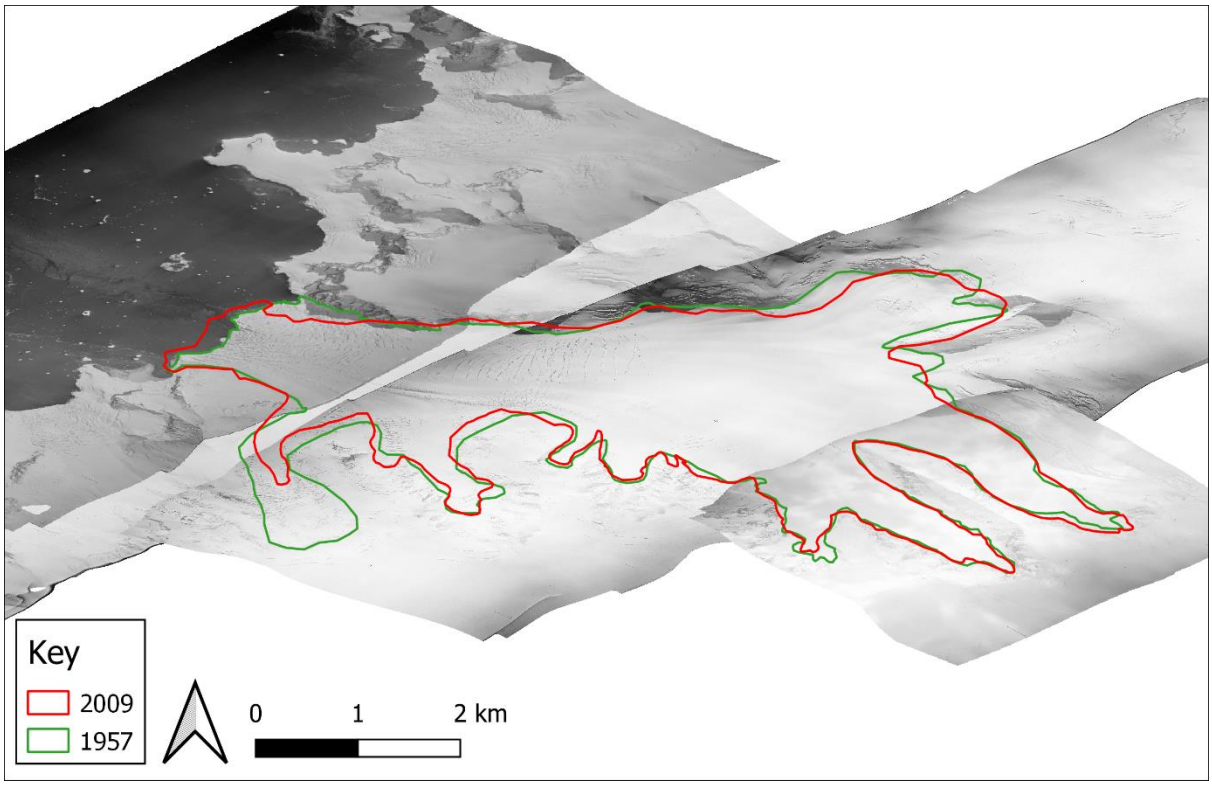

Figure 21. Change in Leonardo area extent from 1957-2009 overlying 1957 BAS orthomosaic.

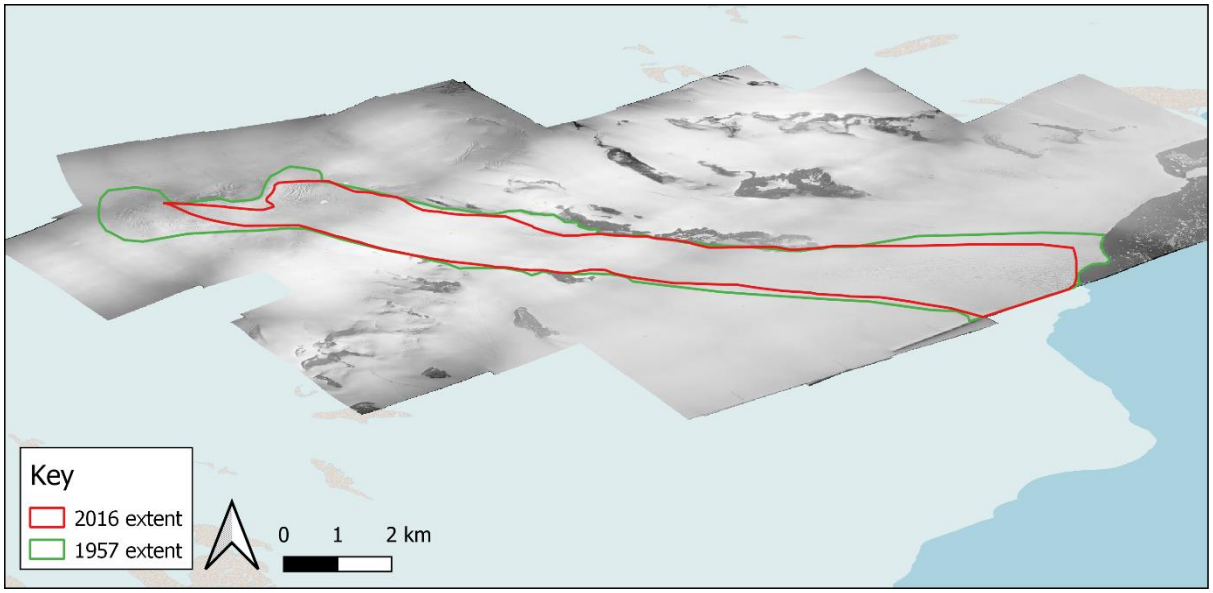

Figure 22. Change in Diplock area extent from 1957-2016 overlying 1957 BAS orthomosaic and OpenStreetMap Basemap.

The combination of shrinking and thinning results in a change in glacier shape and slope profile, with Leonardo's average slope levelling as it thins at the head, and Diplock steepening as it thins at the terminus (Figure 17 and 20). The slope percentage for each DEM is outlined in the table below and was calculated as the change in altitude over distance, from head to terminus (USGS 2023).

Table 11. Slope profile of Leonardo and Diplock centre lines.

	Leonardo		Diplock	
	1957	2009	1957	2016
Change in Altitude	500.02 m	-195.63 m	1167.13 m	1458.11 m
Distance	7483.45 m		16480.23 m	
Slope Percentage	6.68%	-2.61%	7.08%	8.85%

4.3 Summary

Whilst Leonardo and Diplock have opposing aspects and are of a similar size, they are located at slightly different latitudes and vary in their shape and characteristics. This is a limitation when comparing their response over time as the characteristics of a glacier contribute greatly to their behaviour as will be discussed in the following section. Overall, these results show that both Leonardo and Diplock lost significant mass during the observed period, with westward facing Leonardo thinning significantly more than eastward facing Diplock as expected. This indicates there is a relationship between mass loss and aspect, the significance of which is discussed in section 5.3. The accuracy and precision of each DEM is summarised in Table 12, whereby MAE is used to measure accuracy, RMSE vertical accuracy, and SD precision (Papworth 2014).

Table 12. Summary of the accuracy and precision of DEMs created from both BAS archived film photographs and Icebridge aerial photography.

	Leonardo		Diplock	
	1957	2009	1957	2016
Root Mean Squared Error (RMSE)	5.13 m	6.98 m	7.50 m	7.54 m
Mean Absolute Error (MAE)	5.65 m	7.79 m	7.02 m	7.78 m
Standard Deviation Absolute Error (SD)	2.37 m	3.49 m	2.66 m	1.98 m

Table 13. Summary similarities and differences in observed changes.

Observed changes	Similarities	Differences
Elevation	Leonardo: 1618.82m of elevation lost between 1957-2009. Diplock: 349.59m of elevation lost between 1957-2016.	Leonardo: Greatest loss at glacier head and slight gain along the tongue. Unknown value for terminus. Diplock: Greatest loss at glacier terminus and slight gain at the glacier head.
Shape and size	Leonardo: Lost 2,943.32 m^2 of surface area at a rate of -56.60 m^2 p.a. Diplock: Lost 10,250.51 m^2 of surface area, at a rate of -174.25 m^2 p.a.	Leonardo: Thinning and shrinking led to decrease in average slope angle but increase in slope variation. Diplock: Thinning at the terminus led to an increase in average slope angle.

5.0 Discussion

As summarised in Table 13, both Leonardo and Diplock lost mass over the period measured with Leonardo thinning fastest, at a rate of -31.12 m p.a., and Diplock shrinking fastest, -174.25 m^2 p.a. With measurements of Antarctic Peninsula glaciers dating back to the 1940s, general trends for the region show that 90% of marine-terminating glaciers have lost mass, with differences observed on the east and west coasts of the Peninsula (Davies et al. 2012; Cook 2014). The following section will discuss the changes outlined in Table 13, compared to those observed regionally, whilst focusing on the significance of aspect regarding observed changes.

5.1 Observed Changes in Leonardo and Diplock

Thinning and shrinking of marine terminating glaciers is associated with dynamic instability (Meier et al. 2007). Whilst both glaciers thinned over the period monitored, Leonardo lost significantly more than Diplock, approximately 29.4% of its elevation. Leonardo is the

smaller of the two glaciers with an extent of approximately 25km^2, composed of multiple valley glaciers which flow into a single westward facing basin (Rau et al. 2005). Additionally, Leonardo has a cascading longitudinal profile, which varies in percent of slope (Rau et al. 2005). Huber et al. (2017) found that mean thickness varied with area and slope, with steeper, smaller glaciers, being thinner. Whilst the percent of slope following Leonardo's centre line is less than that of Diplock, Figure 17 shows how the glacier surface does not flow gently down slope but rather rises as it flows down the tongue. In addition, Leonardo's tongue did not change much in elevation, and is classified as stationary by GLIMS (Table 7). This could be because the glacier tongue is surrounded by steep rocky outcrops whereby accumulation may occur, or as the result of narrowing at the tongue, forcing the ice to occupy more space vertically, or the result of bumps in the bed topography, characteristic of cascading longitudinal profiles (Rau et al. 2005). The lack of thinning along the tongue compared to that at the head is most likely the result of a combination of all three, which would also allude to the observed thinning at the head, being steep and relatively small in area, this in addition to Leonardo's westward slope profile discussed in section 5.3 (Huber et al. 2017).

Table 14. Rate of change in elevation, thinning, per year for Leonardo and Diplock as shown in section 4.1 and 4.2.

Rate of change per year	Leonardo	Diplock
Thinning	-31.12 m	-5.93 m
Shrinking	-56.60 m^2	-174.25 m^2

Leonardo and Diplock are both classified as outlet, or marine-terminating glaciers, by GLIMS, with Diplock previously being a tributary glacier feeding into the Prince Gustav Ice shelf prior to its collapse in 1995 (Rau et al. 2005; Davies 2020b). Glasser et al. (2011) observed the collapse of the Prince Gustav Ice Shelf before and after, in addition to the rapid shrinking and thinning of tributary glaciers that subsequently followed (Glasser et al. 2011). Diplock lost 3.1% of its elevation over the observed period, significantly less than Leonardo. However, both glaciers lost similar volumes of mass as outlined in Table 15, with Diplock loosing mass at the terminus via thinning at a rate of -5.93 m p.a., and surface area at a rate of -174.25 m^2 p.a. (Table 14). Furthermore, Diplock has an even, longitudinal profile, which has steepened because of thinning at the terminus (Figure 20) (Rau et al. 2005). Pastik et al. (2021) observed longitudinal slope on marine terminating glaciers to be the connecting factor

between front position and glacier thickness, with steeper slopes resulting in greater mass loss and frontal retreat as observed in Figures 19 and 20 (Huber et al. 2017). This is because Ice-shelves act as buffers by reducing stress and restricting the rate of flow from its tributary glaciers (Hulbe et al. 2008). The collapse of ice shelves causes the destabilisation of tributary glaciers, with glaciers feeding the Larsen A and Prince Gustav ice shelves, experiencing accelerated mass loss in the years following their collapse (Rott et al. 2002; Hulbe et al. 2008).

Table 15. Estimated volume and change in volume, calculated from distance and the mean elevation of the glacier centre line, Figure 17 and 20, multiplied by polygonised extent shown in Figures 21 & 22.

Volume	Leonardo	Diplock
1957	0.02565 km^3	0.03384 km^3
2009/2016	0.01620 km^3	0.02476 km^3
Difference	0.00945 km^3	0.00908 km^3

5.2 Observed Changes on the Antarctic Peninsula

As discussed in section 5.1, the observed differences in Leonardo and Diplock's elevation over the period measured are not unique to them, but rather well documented spatial variations observed along the east and west coasts of the Antarctic Peninsula. Figure 7 shows the accelerating rate at which mass is being lost in Antarctic, with interannual fluctuations on the Peninsula, found to be correlated to oscillations in annual Positive Degree-Days (Pudelko et al. 2018). Thus, whilst mass loss on the Antarctic Peninsula is unanimous, locally, and interglacially, huge variations in response exist (Pudelko et al. 2018).

Previous work by Cook 2014; and Huber et al. 2017, shown in figure 23, produced a hypsometric curve of glaciers on the Antarctic Peninsula, used to show the distribution of elevations across the Peninsula using data from the GLIMS World Glacier Inventory (WGI) (Figure 25). Huber et al. (2017) state that the bimodal shape of the curve is the result of the unique topography of the Antarctic Peninsula, whereby the central ridge divides the Peninsula into east and west facing slopes. Most of which are valley glaciers, with large altitudinal ranges (Huber et al. 2017). Subsequently, the elevation of marine-terminating and tributary glaciers reflects the topography of the Peninsula. Glaciers on the west coast are

limited by their surrounding topography which is characterised by steep increases in elevation towards the ridge, steep ice-free slope, and rocky outcrops (Benn and Evans 1998; Huber et al. 2017). Conversely, east coast glaciers are subject to gentler topography, resulting in vast expanses of low-lying tributary and marine-terminating glaciers (Huber et al. 2017). As stated by Huber et al. (2017), 63% of the Peninsula drained by marine-terminating glaciers, and 35% by tributary glaciers. As shown in Figure 23a, the greatest glaciated area is only a few hundred meters above mean sea level, with median elevation increasing towards the interior ridge (Huber et al. 2017). As a result, most glaciated areas are only a few hundred meters relative to mean sea level, which means even a slight rise in the ELA will result in a huge loss of mass (Huber et al. 2017).

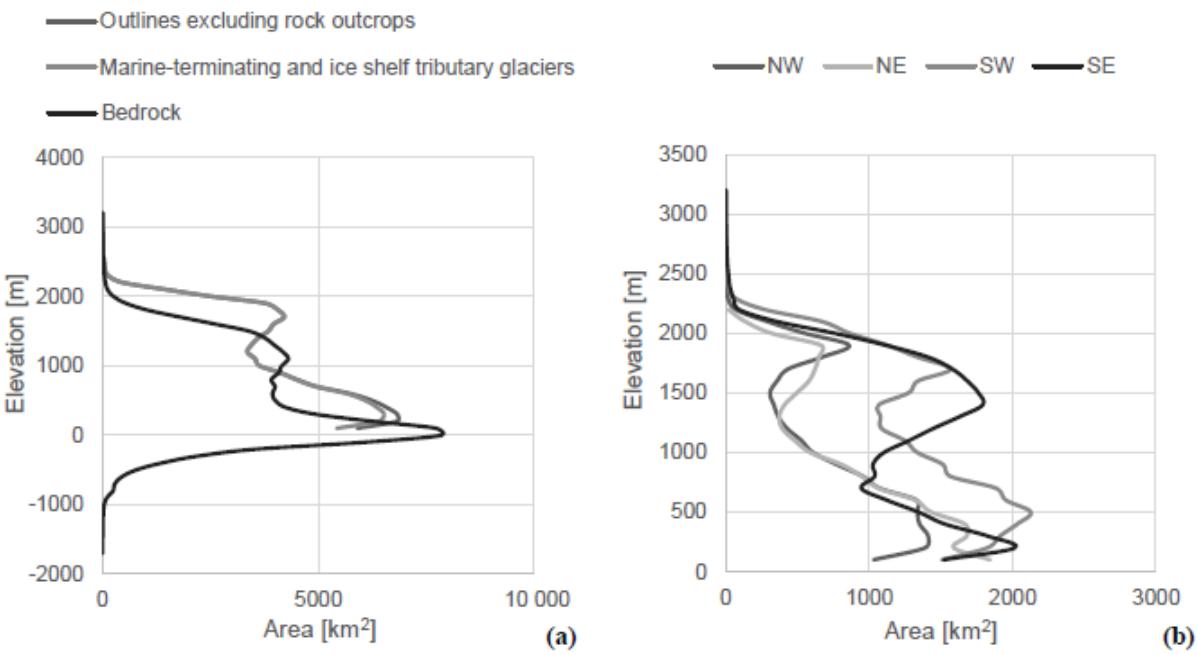

Figure 23. Glacier hypsometry of the total area on Antarctic Peninsula covered by Cook et al. (2012) DEM using classifications from GLIMS. (a) Total area distribution. (b) Distribution of glacier area on Antarctic Peninsula per sector, Northwest (NW), Northeast (NE), Southwest (SW), and Southeast (SE) (Cook et al. 2012; Huber et al. 2017).

Figure 23b, shows the distribution of glacial coverage per sector with NE and NW glaciers covering much smaller areas compared to those in the SW and SE sectors (Huber et al. 2017). Whilst this distribution can be mostly attributed to the topography of the Peninsula, glaciers on the Northern Antarctic Peninsula have been observed to be particularly vulnerable to climate change. Davies et al. (2012) observed Northern Antarctic peninsula glaciers from 1988-2001 and found east coast glaciers to be shrinking at a rate of -0.35% p.a., comparable

to the rate shrinking observed for Diplock, -0.41% p.a. from 1957-2016. Conversely, Davies et al. (2012) observed reduced shrinking on the west Northern Antarctic Peninsula, at a rate -0.20% p.a., consistent with the rate of shrinking measured for Leonardo, -0.20% p.a. from 1957-2009. Furthermore, Davies et al (2012), observed a greater reduction in thickness on the west coast, which highlights the relationship between mass loss and topography. Scambos et al. (2014) attribute the observed variations in mass balance on the east and west coasts of the Antarctic Peninsula to be the result of a combination of the following changes: Inland retreat along western coastal fjords, ice shelf loss along the eastern coast, widespread and accelerating inland retreat along the eastern coast, and an increase in snow accumulation along the western coast. Each of which will be discussed in the following paragraphs.

Inland retreat observed along the Western Antarctic Peninsula is partly attributed to extensive fjords which have varying responses to climate change (Grange and Smith 2013). As previously discussed, the peninsula is divided in two by the ridge of the Transantarctic mountains, which also extend across the continent, dividing East and West Antarctica (Hale 2014). Most glaciers on the Antarctic Peninsula are valley glaciers, which are strongly influenced by bedrock lithology and structure (Benn and Evans 1998; Huber et al. 2017). The Western Antarctic Peninsula is composed of 674 fjord glaciers, of which 216 are losing mass (Pineda-Metz 2021). Lundergaard et al. (2018) investigated Andvord Bay, a fjord located 15km south of Leonardo, and observed its tidewater glaciers to remain stable despite persistent warm ocean temperatures (Cook 2014). Additionally, most of the mass loss in Andvord Bay was lost via carving, much like Leonardo, outlined in Table 7 (Rau et al. 2005; Lundergaard et al. 2018). Due to the varying topography along the west coast resulting from fjords and low-lying valley glacier systems, Davies et al. (2012) found marine-terminating glaciers to be shrinking at varying rates, which they propose is likely the result of carving processes. Leonardo's terminus shows little change over the period measured (Figure 21) but thinned significantly at the glacier head, likely due to aspect and slope angle resulting in increased exposure to solar radiation. Thus, whilst the position of the terminus remained stable, significant mass was lost during the period, potentially via increased carving (Mohodt et al. 2017). Furthermore, with rising ocean temperatures, marine-terminated glaciers are expected to continue losing mass, with fjords vulnerable to meltwater and sediment inputs, which could lead to the destabilisation of their glaciers (Grange and Smith 2013; Huber et al. 2017). Cook (2014) concludes that persistent warm ocean temperatures are the primary cause of mass loss on the west coast. However, the complexity of ice-ocean interactions is beyond

the scope of this project but is recognised to be responsible for increased carving on the Western Peninsula. However, the role of aspect on localised changes, such as those observed at Leonardo's glacier head, is significant and discussed in greater detail in section 5.3.

The thinning and retreat of ice shelves is well documented and known to cause the destabilisation of tributary glaciers, resulting in accelerated mass loss (Seehaus 2021). Seehaus (2021) argues this is the main driver of the observed increase in mass loss from the Antarctic Peninsula from 1997-2017, whereby an additional 26±16 Gt p.a. was lost. Glaciers along the Eastern Antarctic Peninsula have changed considerably over the past decades following the collapse of several ice shelves since 1995 (Seehaus 2021). Davies et al. (2012) investigated glaciers on the Trinity Peninsula, at the northernmost tip of the Antarctic Peninsula, and observed the fastest shrinking glaciers to be ice-shelf tributary glaciers, such as Diplock. Conversely, the observed retreat of tributary glaciers on the Western Peninsula is contrasting to that of the East. Rignot and Thomas (2002) observed, no ice-flow changes after the collapse of the Wordie Ice Shelf in Western Palmer Land. Whereas retreat in the 4 years following the collapse of the Larsen Ice Shelf was threefold that observed following the loss of the Wordie Ice Shelf (Rignot and Thomas 2002). Seehaus et al. (2018) observed a loss of 238.81 km^2 of glacier extent between 1985-2015, of which 208.59 km^2 is attributed to ice shelf disintegration, the majority of which was lost along the east coast. However, east coast glaciers feeding the former Prince Gustav Ice Shelf, receded by only 21.07 km^2 from 1985–2015, and decelerated 58% on average from 1992–2014 (Seehaus et al. 2018). This highlights the large uncertainties surrounding the future contribution of east coast tributary glaciers to total mass loss on the Peninsula due to the variation in observed rates of retreat. Furthermore, the rate of change shown in table 14 is averaged over 59 years and therefore is not representative of the variance in rate of change following ice shelf collapse. In addition to ice shelf collapse on the east coast, non-ice shelf tributary glaciers also show considerable loss of mass despite eastern aspects receiving less solar radiation (West and Howard 2019; Seehaus 2021). Thus, more analysis is necessary to infer correlations between aspect and mass loss on the Eastern Peninsula (Seehaus 2021).

In addition to ice-ocean interactions, Scambos et al. (2014), attribute the Western Peninsulas marine-terminating glaciers reduced contribution to total mass loss to be because of an increase in snowfall. Ice core records from 1801-2010 show an increase in precipitation during the 20th century, with snowfall on the west coast equivalent to >3000mmw.e. p.a. (mm water equivalent), and <500mmw.e. p.a. on the east (Thomas et al. 2017). Broeke et al.

(2006) and Davies et al. (2012), attribute greater accumulation on the West Peninsula to result from steep topography, with ice free slopes, and rocky outcrops, acting as sources of snow and ice via avalanches and snow drift (Benn and Evans 1998). Additionally, the rapid increase in elevation towards the ridge on the Western Peninsula, results in a rapid decrease in temperature with distance, and subsequently greater accumulation (Turner et al. 2005). Whilst topography plays a key role in the accumulation gradient from West-East, Thomas et al. (2017) discusses the role of surface moisture, with greatest changes in accumulation found in ice cores obtained from the South-West Peninsula. The core revealed a doubling of accumulation since the 1850s, with acceleration in recent decades (Thomas et al. 2008). By comparing accumulation records with atmospheric circulation variability, Thomas et al. (2008) found a strong positive relationship between the Southern Annular Mode (SAM) and mass balance. As defined by the Bureau of Meteorology (2023), SAM refers to the north-south migration of strong westly winds in the mid- to high-latitudes of the southern hemisphere, resulting from changes in air pressure on a timescale of 10s to 100s of years' (Davies 2023). Turner et al. (2005) also attributes observed inter-decadal changes in temperature, pressure, and wind speed, to SAM. During a SAM negative phase, the Peninsula cools and there is greater accumulation, and during a positive phase, temperature increases, and greater mass is lost (Davies 2023). Subsequently, SAM has a big influence on precipitation patterns on the Antarctic Peninsula, which is observed to be stronger on the Western Peninsula (Thomas et al. 2017; Turner et al. 2020). SAM is currently in a positive phase, furthermore, this phase is predicted to continue due to increased greenhouse gas emissions, as the system is closely linked to the upwelling of Circumpolar deep water and subsequent CO_2 degassing (Davies 2023). Thus, SAM is predicted to remain in a positive phase for some time, driving continued mass loss on the Western Peninsula despite increased accumulation.

To summarise, this section discussed the observed changes in mass on the east and west coasts of the Antarctic Peninsula compared to those observed for Leonardo and Diplock. Additionally, the behaviour of various tributary and marine-terminating glaciers was examined to provide insight into the complexity of glacial behaviour. The significance of which aspect plays on the change in glacial thickness is discussed in the following section.

5.3 The Significance of Aspect

As shown in Figure 24, >25% of glaciers on the Antarctic Peninsula as identified by the WGI are westward facing, compared to <10% eastward facing (Cook 2014). In addition, Figure 25, shows the distribution of glaciers on the Antarctic Peninsula as identified by the GLIMS WGI. As highlighted by Cook (2014), there are less marine-terminating glaciers on the east coast of the peninsula than on the west, with substantially more tributary glaciers due to the low-lying topography (Huber et al. 2017). In addition, Huber et al. (2017) investigates the relationship between mean elevation and mean aspect on the Antarctic Peninsula and found no significant regional trends (Cook 2014). However, the role of aspect locally has yet to be investigated thoroughly but is predicted to be more significant locally than regionally, especially when investigating complex glacier systems such as those on the Antarctic Peninsula (Benn and Evans 1998; Cook 2014; Geçen et al. 2018).

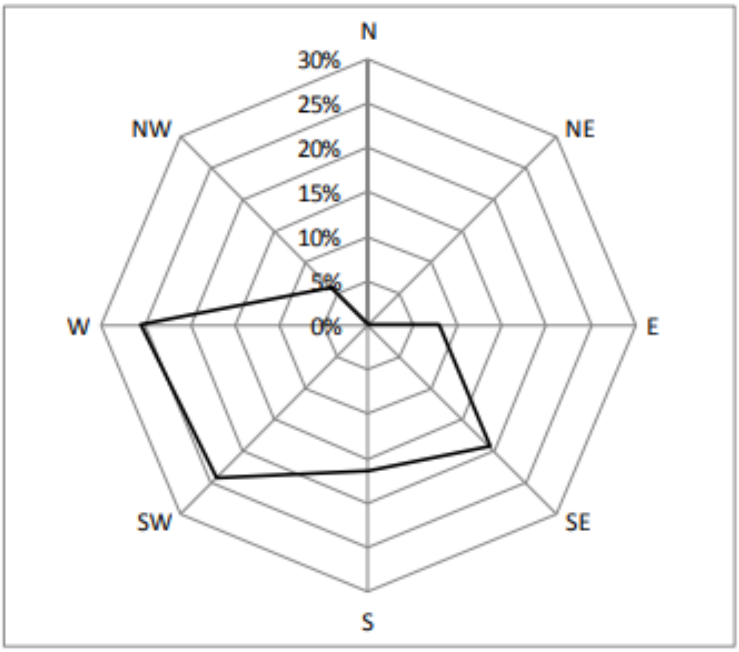

Figure 24. The percentage of all marine-terminating glaciers identified by the WGI on the Antarctic Peninsula (Figure 25) within each aspect sector, where the aspect value for each glacier is the mean value for the whole basin (Cook 2014). Obtained from Cook (2014).

Due to the axis and orbit of the earth, the Northern hemisphere receives more solar radiation, also known as insolation, with highest insolation received at the equator (Earth Observatory 2009). As a result, glaciers are more extensive at extreme latitudes as shown in Figure 1, due to the low solar angle, resulting in less insolation per m^2 (Figure 26) (Benn and Evans 1998). The Antarctic zone (60°-75°S) has very large seasonal variations in solar radiation, resulting

in winter accumulation and summer ablation (Geography 2023). Zeng et al. (2022) calculated the monthly average daily solar radiation value of the Antarctic Peninsula to be highest in the austral summer, December-February, at 12.58 MJ m^{-2}, and lowest during austral winter, June-August, 1.06 MJ m^{-2}.

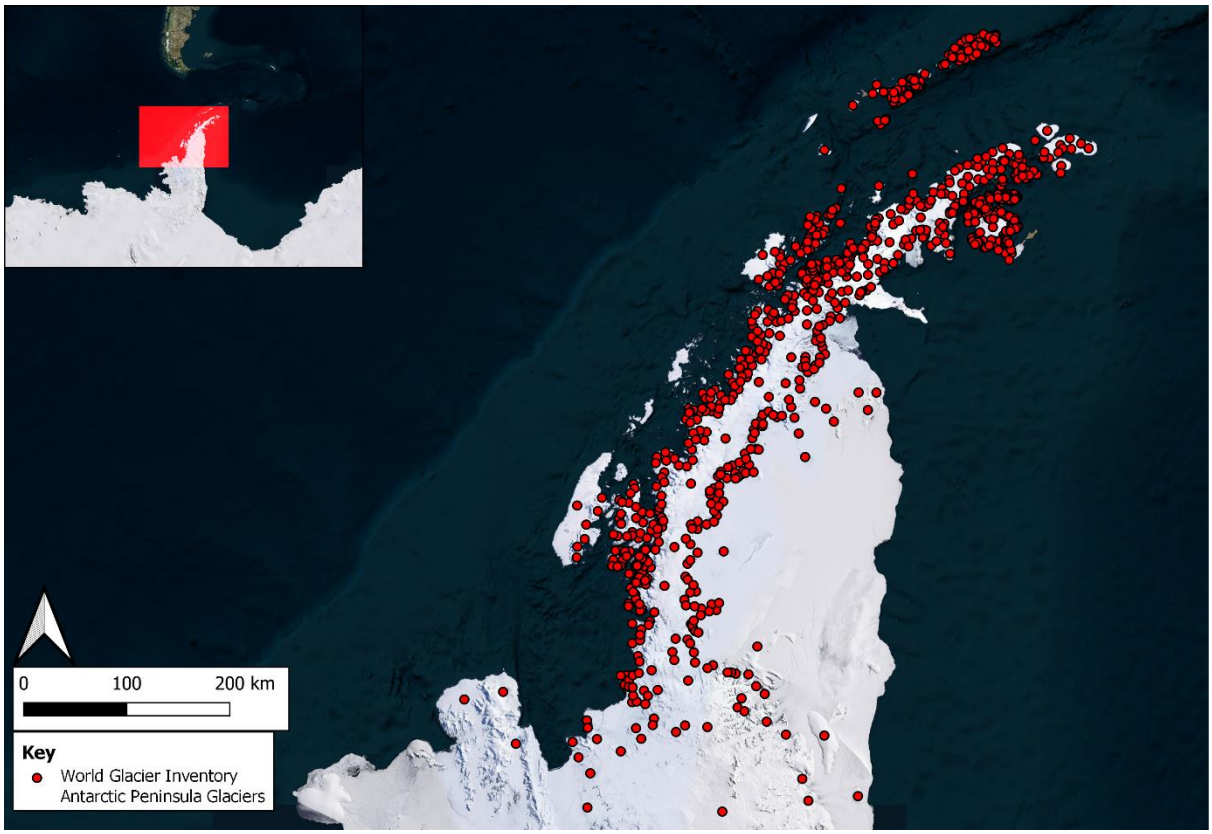

Figure 25. The distribution of glaciers on the Antarctic Peninsula identified by GLIMS WGI obtained from the National Snow and Ice Data Centre (NSIDC), overlying Bing Virtual Earth Basemap with wider extent shown in the in-picture map, top left (NSIDC 2022).

In the Southern Hemisphere south facing slopes receive less insolation than north facing slopes (West and Howard 2019; Kunaka 2020). As discussed previously, Davies et al. (2012), found glaciers on the Northern Antarctic Peninsula to be shrinking fastest which could be attributed to their aspect and latitude, as the amount of insolation increases towards the equator. The variation in insolation received by east and west aspects is more nuanced than north and south as it varies with time of day. West facing slopes receive the most insolation in the afternoon when temperatures are higher, and East facing slopes in the morning, when temperatures are lower (West and Howard 2019). This correlates with recorded mean annual temperatures for the region, with the Vernadsky meteorology station on the Western Peninsula measuring -2.9±1.1°C from 1981-2010, compared to -4.6±1.1°C recorded mean at

Esperanza on the Northeast coast (Turner et al. 2020). However, meteorology stations on the Western Peninsula experience some of the largest variability in annual mean temperature resulting from a variation in mean sea level pressure (Turner et al. 2020). The extent to which these effects the mean annual temperature is beyond the scope of this investigation but further highlights the complexity of the Antarctic Peninsula glacier system.

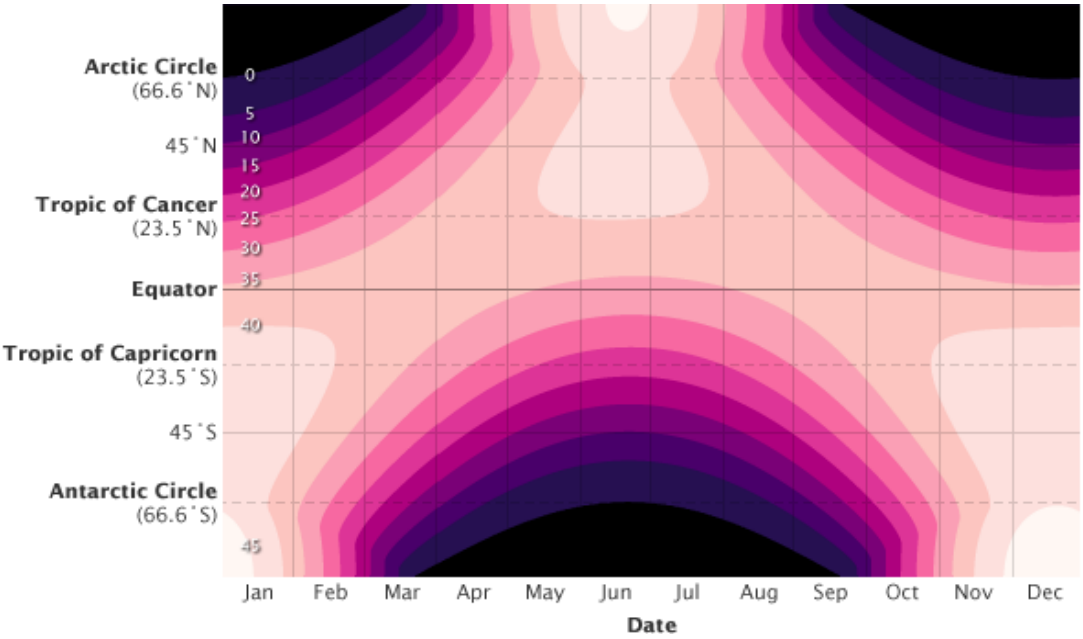

Figure 26. The average daily solar radiation received at the top of the atmosphere at each latitude, where total energy received ranges from 0 MJ m^{-2} per day, shown in black, to 50 MJ m^{-2} per day, pale pink (Earth Observatory 2009). Obtained from NASA's Earth Observatory (2009).

The slope and aspect of a surface determines the amount of insolation received, with surfaces angled towards the source of insolation receiving the most (Bennie et al. 2008). The results of this investigation indicate that westward facing slopes lose more mass via thinning and eastward slopes via shrinking. This is consistent with the literature, linking terminus retreat on the east coast with destabilisation following ice shelf collapse (Rott et al 2002; Hulbe et al; 2008). Seehaus et al. (2018) attribute 208.56km^2 of the 238.81km^2 loss of glacier extent from 1985-2015 to be from ice shelf disintegration (Seehaus et al. 2018). A possible explanation for the greater contribute of eastern glaciers to total mass loss is the role of topography, whereby low-lying areas are more vulnerable to mass loss as ELA rises, despite receiving less insolation (Huber et al. 2017; Seehaus et al. 2018). Additionally, the surrounding topography of Diplock offers little shade and thus is more exposed than Leonardo, which is

surrounded by steep, ice-free slopes (Figure 21). The increased exposure of Diplock also makes it vulnerable to loss of mass via snow drift as the prevailing wind direction is from east to west, dominated by the Polar Easterlies (Discovering Antarctica 2023). However, following the loss of low-lying ablation zones, mass loss of tributary glaciers has been observed to decelerate (Davies et al. 2012; Seehaus et al. 2018). Therefore, the contribution of mass loss from tributary glaciers to total loss across the Peninsula is expected to decline as glaciers steepen and reach a new equilibrium.

As previously discussed, this investigation found westward facing Leonardo to lose the most mass via thinning, and less mass via shrinking, as was to be expected. Westward facing slopes receive most insolation in the afternoon when temperatures are highest and subsequently expected to lead to increased mass loss (West and Howard 2019; Turner et al. 2020). Despite the loss of mass via thinning, the change in surface area was small and most likely due to the rigid topography which limits glaciers extent to their valley basins. Additionally, the varying slope angle of Leonardo indicates increased mass loss via carving whilst still maintaining terminus position, resulting in loss of elevation (Mohodt et al. 2017). However, mass may still be lost via sublimation, snow drift and surface melting. Leonardo thinned most at the head, which has a large surface area and less sheltered by ice free slopes and rocky outcrops resulting in increased exposure to insolation for a longer period throughout the day (Figure 16). Thinning at the glacier head may also be the result of compaction from seasonal surface melting and refreezing and has been found to contribute significantly to mass balance (Pelt et al. 2016). Pelt et al. (2016) attribute this to refreezing being substantially smaller than the amount of refreezing, as air trapped within glacier ice is lost during melt and thus refrozen meltwater is far denser. This coupled with the complex ice ocean interactions occurring at the terminus and persistent warm ocean temperatures provides an insight into the observed changes in mass of Leonardo from 1957-2009 (Cook 2014). However, more investigation is required to better understand the extent to which aspect and warm ocean temperatures contribute to the observed changes.

The patterns and significance of circulatory systems that contribute to atmospheric and ocean temperature gradients are beyond the scope of this research. However, the uneven distribution of solar radiation, around the globe is a key contributor to these systems. Linacre and Geerts (1999), and Stanhill and Cohen (1997) observed a decrease in the annual solar

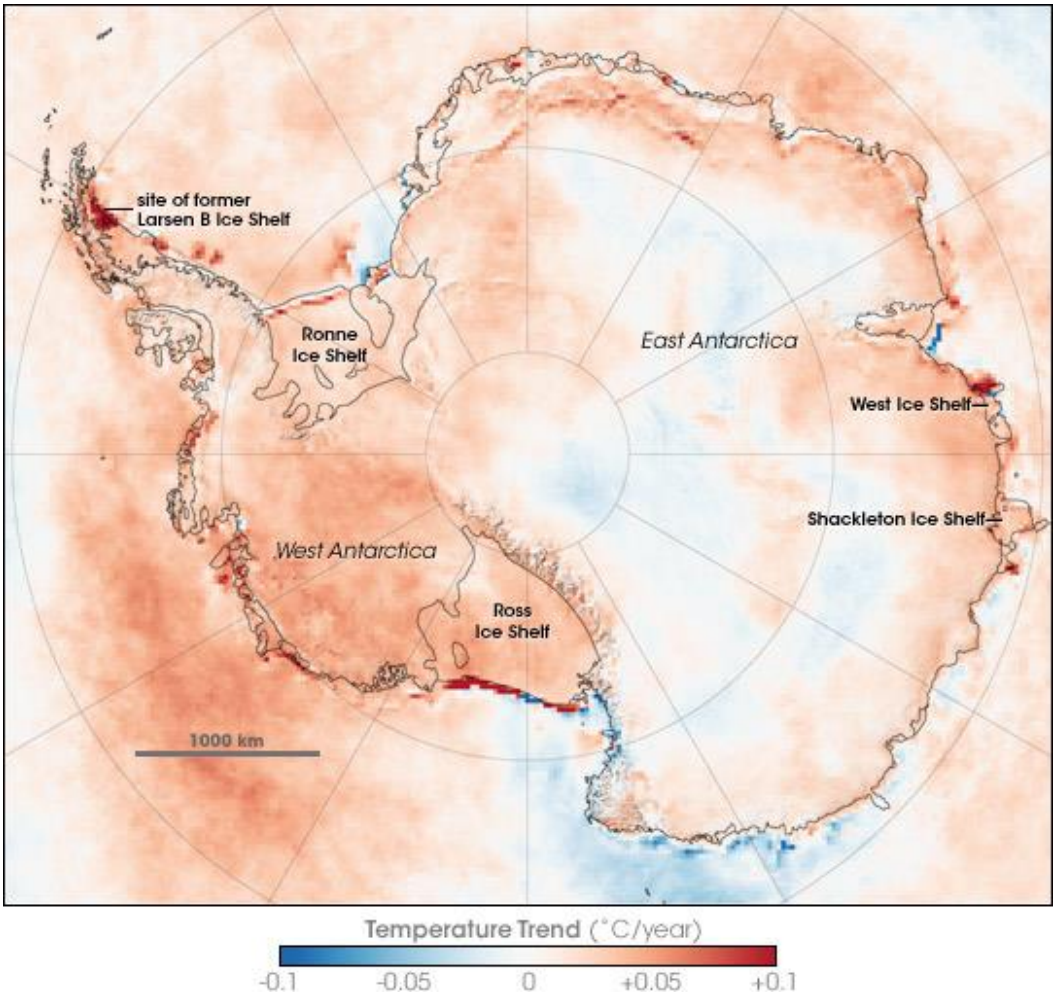

Figure 27. Two Decades of Temperature Change in Antarctica, 1981-2007 (Simmon 2007), obtained from NASA earth observatory.

radiation reaching Antarctica, averaging -0.28 W m^{-2} per year from 1959-1988. The reason for this decline is unclear but is greater than can be attributed to errors in pyranometer measurements (Stanhill and Cohen 1997). One possible explanation proposed by Stanhill and Cohen (1997), is an increase in aerosol concentrations, with some stations reporting increased haziness, resulting in less solar radiation reaching the surface, as well as a reduction in longwave radiation loss, resulting in atmospheric warming (Linacre and Geerts 1999; Bai et al. 2022). The Antarctic Peninsula has reportedly experienced regional warming six times that of the global average over the last century (Vaughan et al. 2001). This warming has resulted in a 10-fold increase in glacier flow and rapid ice sheet retreat, facilitated by surface and bottom melting (Scambos et al. 2000; Shepherd et al. 2003; Rignot 2006). In their study of Antarctic climate change, Turner et al. (2005), found the Antarctic Peninsula to have experienced increased warming over the last 50 years, with average air temperatures in the northern peninsula rising by 2.5°C from 1950-2000. Temperatures recorded at the Faraday

station, located south of Leonardo on the west coast, increased at a rate of 0.56°C decade^{-1} averaged over the year, and 1.09°C decade^{-1} during the winter, indicating additional inter-annual fluctuations (Turner et al. 2005). Temperatures observed by Turner et al. (2005), are far higher than the global average of 0.6°C per century (Davies et al. 2012). Additionally, Antarctic peninsula glaciers have a higher potential contribution to global sea level, 54mm, compared to the glaciers of Alaska (45 mm), and Central Asia (10mm) (Huber et al. 2017). Further indicating the importance of investigating Antarctic Peninsula Glaciers.

5.4 Limitations

Limitations of this investigation are extensive, primarily due to the lack of high spatial resolution data available for the study area, incomplete camera calibration reports, and complications associated with utilising archived aerial film photography.

Due to the incomplete coverage of Icebridge aerial photographs for both Leonardo and Diplock, the area extent was measured using part orthomosaics and part supplementary Landsat imagery, with a spatial resolution of 30m. Landsat 7 imagery obtained in 2009 was used to supplement the terminus of Leonardo, and Landsat 8/9 imagery obtained in 2016, to supplement the glacier tongue and head of Diplock. Furthermore, due to a lack of time and resources, elevation, and glacier extent were only measured at the start and end of the period. Subsequently variation in the rate of change throughout the period could not be measured. As a result, the rate of change per year outlined in Table 14, is averaged across the period, and not representative of the actual inter-annual, annual, or decadal variations in mass. In addition, the terminus of Diplock was partly missing from 1957 aerial photos, so to maintain consistency the same terminus extent was measured over both periods. Due to the extent of incomplete coverage by Icebridge aerial photographs of Diplock, a DEM was created using the available Icebridge imagery and then merged with Cop-30m DEM in GIS. Cop-DEM was chosen due its high-vertical accuracy. Which, according to Copernicus (2017), has a vertical resolution of 1m and accuracy of 7m, in alignment with the accuracy observed by Ghannadi et al. (2023), discussed in section 1.2.2 and 3.3.

Incomplete coverage of Icebridge airborne Lidar data resulted in it being necessary to use Cop-30m DEM to identify elevations of GCPs. The accuracy and precision of each DEM is outlined in Table 12, with the most accurate built using 1957 BAS aerial photographs of Leonardo (Figure 15). This is likely due to the additional GCPs used as reference in the

photogrammetric software. Due to unknown pixel sizes, fiducial coordinates, and multiple flight paths, reference data was relied upon to correctly align the photographs. However, despite the additional GCPs, once merged there was not enough overlap between different flight lines to generate a DEM or orthomosaic with complete coverage of Leonardo from the 1957 BAS Aerial photographs. Additionally, a potential source of bias during the study is the influence of the data analyst on the observed error for each GCP. Furthermore, the accuracy and precision outlined in Table 12 does not consider the accuracy and precision of other products used for identifying GCPs.

6.0 Conclusion

The purpose of this investigation was to assess the significance of aspect on observed multi-decadal changes in glacial thickness of marine-terminating glaciers on the Antarctic Peninsula. This is the first study of substantial duration which examines associations between aspect and glacial thickness at extreme latitudes. The findings clearly indicate a variation in glacial behaviour and morphology on the Antarctic Peninsula of those with eastward facing aspects compared to westward facing aspects. As expected, Leonardo thinned significantly more than Diplock over the period, despite regional mass balance measures attributing the increased negative regional mass balance to the retreat of tributary glaciers on the east coast. In addition to measuring change in elevation, this investigation highlights the change in glacier shape and discussed the relationship between slope profile and mass balance. These findings provide additional evidence for the deceleration of tributary glaciers in the years following ice shelf collapse and provide important insights into the potential future contribution of westward facing marine-terminating glaciers to regional mass balance. Despite previous work by Huber et al. (2017) finding no significant relationship between aspect and mean elevation regionally, there is a clear spatial variation in mass loss across the peninsula attributed to east and westward facing aspects. One of the strengths of this study is that it links observations with regional trends, thereby highlighting the usefulness of this work in understanding local and regional glacier dynamics. Furthermore, analysis of atmospheric and ocean temperatures indicates a strong relationship between change in glacier thickness on the west of the Peninsula and ocean temperature patterns (Cook 2014). This is the result of the complex interactions between ice, ocean, atmosphere, and local topography, which significantly contribute to glacier behaviour and are still not fully understood.

Therefore, whilst aspect plays an important role in glacial morphology, the relationship between glacial thickness and aspect is only significant when investigating individual glaciers. The application of this method for larger areas requires the consideration of a considerable larger number of variables and their interactions with each other. Additionally, the findings of this investigation have limited application for glaciers located at different latitudes due to the relationship between latitude and insolation. Thus, whilst these results are not applicable regionally, they provide insight into the complexity of glacial behaviour on the Antarctic Peninsula and highlight the potential usefulness of high resolution archived aerial photography in measuring multi-decadal changes in elevation. Furthermore, this investigation highlights the need for more high spatial resolution imagery to provide geographic references and support archived aerial photographs, thereby enabling more detailed analysis of glacial response to climate change over long periods.

7.0 Recommendations

More research is needed to develop a deeper understanding of the relationship between Aspect and Glacier thickness. Little work has been done on the role of aspect on glacier mass balance, with most studies spanning decades focusing on large areas, and assessing regional changes in elevation and mass balance, thus overlooking the nuances in glacier behaviour. Additionally, the push for global glacier monitoring favours satellite-based systems and thus despite the high accuracy and precision of airborne systems, there is a lack of available airborne data for glaciated regions such as the Antarctic Peninsula. This is primarily due to the increased cost and time needed to fly aircraft up and down the peninsula, but also limited by the inaccessible nature of many glaciated areas at extreme latitudes. The DEMs created as part of this investigation have varying accuracy and precision comparable to that of Cop-30m DEM, limited by availability of supporting datasets. To better understand the spatial distribution of elevation, change within each glacier extent was measured. This was used to quantify the change in shape, size, and slope profile over time, in addition to providing scope to measure change in volume. To conclude, aspect was found be significant locally for small areas, in addition to playing a role in regional changes in glacier thickness on the Antarctic peninsula. However, due to complexities discussed in the report, more work must be done to investigate the role of aspect on regional mass balance and highlights the need for high-spatial resolution imagery and geographical reference data. In the future, it will be beneficial

to explore the use of unmanned aerial vehicles (UAVs) for collecting high spatial resolution imagery to monitor changes in glacial mass balance. Being unmanned, UAVs are a much more effective way of obtaining airborne datasets and overcome many of the limitations of using aircraft. Furthermore, by increasing the availability of high spatial resolution datasets of the Antarctic Peninsula, archived aerial photographs, as an underused resource, can be better utilised to produce long-term records of glacial mass balance. In turn this will enable researchers to determine the effectiveness of using archived aerial photographs to build DEMs as opposed to using existing DEM products. Future work would include monitoring multiple glaciers within a region, and potentially multiple regions, to determine the significance of aspect at a regional level to further enhance our understanding of glacier behaviour in response to climate change.

8.0 References

Anagnostopoulos, C., 2023. *What is an Intervalometer?* [online]. PetaPixel. Available from: https://petapixel.com/what-is-an-intervalometer/ [Accessed 23rd April 2023].

Autodesk., 2023. *What is photogrammetry?* [online]. Available from: https://www.autodesk.co.uk/solutions/photogrammetry-software [Accessed 15th April 2023].

Bai, J., Zong, X., Lanconelli, C., Lupi, A., Driemel, A., Vitale, V., Li, K., and Song, T., 2022. Long-Term Variations of Global Solar Radiation and Its Potential Effects at Dome C (Antarctica). *International Journal of Environmental Research and Public Health* [online], 19 (5), 3084.

Benn, D.I., and Evans, J.A., 1998., *Glaciers and Glaciation*. New York: Arnold Publishers.

Bennie, J., Huntley, B., Wiltshire, A., Hill, M.O., and Baxter, R., 2008. Slope, aspect, and climate: Spatially explicit and implicit models of topographic microclimate in chalk grassland. *Ecological Modelling* [online], 216 (1), 47-59.

Braithwaite, R.J., 2017. Can the Mass Balance of a Glacier be Estimated from its Equilibrium-Line Altitude?. *Journal of Glaciology* [online], 30 (106).

Braithwaite, R.J., and Raper, S.C.B., 2009. Estimating equilibrium-line altitude (ELA) from glacier inventory data. *Annuals of Glaciology* [online], 50 (53), 127-132.

Broeke, M., Berg, W.J., Meijgaard, E., 2006. Snowfall in coastal West Antarctica much greater than previously assumed. *Geophysical Research Letters* [online], 33 (2).

Bureau of Meteorology., 2023. *Southern Annular Mode and the Australian climate* [online]. Australian Government Bureau of Meteorology. Available from: http://www.bom.gov.au/climate/sam/ [Accessed 20th March 2023].

Cook, A.J., Murray, T., Luckman, A., Vaughan, D.G., and Barrand, N.E., 2012. A new 100-m Digital Elevation Model of the Antarctic Peninsula derived from ASTER Global DEM: methods and accuracy assessment. *Earth System Science Data* [online], 4, 129–142.

Cook, A.J., 2014. *Spatial and Temporal Changes in Marine-terminating Glaciers on the Antarctic Peninsula since the 1940s*. College of Science: Swansea University.

Copernicus., 2017. *Overview of Global DEM: Assessment of the current global DEMs and requirements for an updated global DEM*. EG-RPT-EEA-SC1-0023.

Correa-Muños, N.A., and Cerón-Calderón, I.A., 2018., Precision and accuracy of the static GNSS method for surveying networks used in Civil Engineering. *Ingeniería e Investigación* [online], 38 (1), 52-59.

Cox, L.H. and March, R.S., 2004. Comparison of geodetic and glaciological mass-balance techniques, Gulkana Glacier, Alaska, U.S.A. *Journal of Glaciology* [online], 50 (170), 363-370.

Davies, B.J., Carrivick, J.L., Glasser, N.F., Hambrey, M.J., and Smellie, J.L., 2012. Variable glacier response to atmospheric warming, northern Antarctic Peninsula, 1988–2009. *The Cryosphere* [online], 6, 1031–1048.

Davies, B., 2015. *Is volume lost/gain or the mass balance of a glacier over the same period the best indicator of climatic change?* [online]. Frequently Asked Questions, Antarctic Glaciers. Available from: https://www.antarcticglaciers.org/question/volume-lostgain-mass-balance-glacier-period-best-indicator-climatic-change/ [Accessed 19th April 2023].

Davies, B., 2020a. *An introduction to Glacier Mass Balance* [online]. Antarctic Glaciers. Available from: https://www.antarcticglaciers.org/glacier-processes/mass-balance/introduction-glacier-mass-balance/ [Accessed 3rd November 2022].

Davies, B., 2020b. *Antarctic Peninsula Ice Shelves* [online]. Antarctic Glaciers. Available from: https://www.antarcticglaciers.org/glaciers-and-climate/changing-antarctica/shrinking-ice-shelves/antarctic-peninsula-ice-shelves/ [Accessed 20th March 2023].

Davies, B., 2023. *Southern Annular Mode* [online]. Antarctic glaciers. Available from: https://www.antarcticglaciers.org/glaciers-and-climate/changing-antarctica/southern-annular-mode/ [Accessed 20th March 2023].

Dembowski, P., 1968. *Finite geometries* [online]. Ergebnisse der Mathematik und ihrer Grenzgebiete, Berlin: Springer-Verlag, ISBN 3-540-61786-8.

Discovering Antarctica., 2023. Regional Climate Variation and Weather [online]. British Antarctic Survey. Available from: https://discoveringantarctica.org.uk/oceans-atmosphere-landscape/atmosphere-weather-and-climate/regional-climate-variation-and-weather/ [Accessed 4th May 2023].

Dong, Y., Zhao, J., Floricioiu, D., Krieger, L., Fritz, T., and Eineder, M., 2021. High-resolution topography of the Antarctic Peninsula combining the TanDEM-X DEM and Reference Elevation Model of Antarctica (REMA) mosaic. *The Cryosphere* [online], 15 (9), 4421-4443.

Dominguez, R., 2019. *Icebridge IODMS0 Ancillary Document*. California: Airborne Sensor Facility, NASA Ames Research Facility.

European Commission., 2023. *TanDEM-X - Digital Elevation Model (DEM) - Global, 12m* [online]. European Union. Available From: https://data.europa.eu/data/datasets/5eecdf4c-de57-4624-99e9-60086b032aea?locale=en [Accessed 15th April 2023].

Earth Observatory., 2009. *Heating Imbalances* [online]. NASA. Available from: https://earthobservatory.nasa.gov/features/EnergyBalance/page3.php [Accessed 30th April 2023].

Earth Resources Observation and Science (EROS) Centre., 2018. *USGS EROS Archive - Digital Elevation - Shuttle Radar Topography Mission (SRTM) 1 Arc-Second Global* [online]. United States Geological Survey. Available from: https://www.usgs.gov/centers/eros/science/usgs-eros-archive-digital-elevation-shuttle-radar-topography-mission-srtm-1 [Accessed 15th April 2023].

European Space Agency (ESA)., 2023. *How does interferometry work?* [online]. Available from: https://www.esa.int/Applications/Observing_the_Earth/How_does_interferometry_work [Accessed 21st April 2023].

Fischer, A., 2011. Comparison of direct and geodetic mass balances on a multi-annual time scale. *The Cryosphere,* 5 (1), 107-124.

Fox, A.J., and Cziferskv, A., 2008. Unlocking the time capsule of historic aerial photography to measure changes in Antarctic peninsula glaciers. *The Photogrammetric record* [online], 23 (121), 51-68.

Geçen, R., Toprak, V., and Tonbul, S., 2018. The Effect of Aspect on Glaciation: A Case Study of Eastern Black Sea Mountains (Turkey). *Aegean Geographical Journal,* 27 (1), 35-54.

Geography., 2023. *Insolation over the Globe* [online]. Available from: https://geography.name/insolation-over-the-globe/ [Accessed 30th April 2023].

GeoNadir., 2022. *What is photogrammetry?* [online]. GeoNadir. Available from: https://geonadir.com/what-is-photogrammetry/ [Accessed 18th April 2023].

Ghannadi, M.A., Alebooya, S., Izadi, M., and Ghanadi, A., 2023. Vertical Accuracy of Copernicus DEM (Case Study: Tehran and Jam cities). *ISPRS Annals of the Photogrammetry, Remote Sensing and Spatial Information Sciences,* X-4, W1-2022.

Glasser, N.F., Scambos, T.A., Bohlander, J., Truffer, M., Pettit, E., and Davies, B.J., 2011. From ice-shelf tributary to tidewater glacier: continued rapid recession, acceleration and thinning of Röhss Glacier following the 1995 collapse of the Prince Gustav Ice Shelf, Antarctic Peninsula. *Journal of Glaciology* [online], 57 (203), 397-406.

Global Land Ice Measurements from Space (GLIMS)., 2023. *GLIMS: Global Land Ice Measurements from Space Monitoring the World's Changing Glaciers* [online]. Available from: https://www.glims.org/ [Accessed 11th March 2023].

Global Security., 2023. *Chapter 8 aerial photographs* [online]. Available from: https://www.globalsecurity.org/military/library/policy/army/fm/3-25-26/ch8.htm [Accessed 26th January 2023].

Grange, L.J., and Smith, C.R., 2013. Megafaunal Communities in Rapidly Warming Fjords along the West Antarctic Peninsula: Hotspots of Abundance and Beta Diversity. *PLOS ONE* [online], 8 (12), e77917.

Greicius, T., and Hartono, N., 2023.*Gravity Recovery and Climate Experiment GRACE* [online]. Available from: https://www.jpl.nasa.gov/missions/gravity-recovery-and-climate-experiment-grace [Accessed 18th March 2023].

Hale, G., 2014. *East and West: The Geography of Antarctica* [online]. Nasa Earth Observatory. Available from: https://earthobservatory.nasa.gov/blogs/fromthefield/2014/11/19/east-and-west-the-geography-of-antarctica/ [Accessed 1st May 2023].

Hubbard, B., and Glasser, N., 2005. *Field Techniques in Glaciology and Glacial Geomorphology*. Chichester: John Wiley & Sons Ltd.

Huber, J., Cook, A.J., Paul, F., and Zemp, M., 2017. A complete glacier inventory of the Antarctic Peninsula based on Landsat 7 images from 2000 to 2002 and other preexisting data sets. *Earth System Science Data*, 9, 115-131.

Hulbe, C.L., Scambos, T.A., Youngberg, T., and Lamb, A.K., 2008. Patterns of glacier response to disintegration of the Larsen B ice shelf, Antarctic Peninsula. *Global and Planetary Change* [online], 63 (1), 1-8.

Jezek, K. C., J. C. Curlander, F. Carsey, C. Wales, and R. G. Barry. 2013. *RAMP AMM-1 SAR Image Mosaic of Antarctica, Version 2.* Boulder, Colorado USA: NASA National Snow and Ice Data Centre Distributed Active Archive Centre. Available from: https://doi.org/10.5067/8AF4ZRPULS4H [Accessed 21st April 2023].

Jiskoot, H., 2014. *Encyclopedia of Snow, Ice and Glaciers: Tributary Glaciers* [online]. Dordrecht: Springer.

Johnson, C., Affolter, M.D., Inkenbrandt, P., and Mosher, C., 2020. *Glacial Budget* [online]. Salt Lake Community College. Available from: https://geo.libretexts.org/Bookshelves/Geology/Book%3A_An_Introduction_to_Geology_(Johnson_Affolter_Inkenbrandt_and_Mosher)/14%3A_Glaciers/14.04%3A_Glacial_Budget [Accessed 18th April 2023].

Kaser, G., Fountain, A., and Jansson, P., 2003. *A manual for monitoring the mass balance of mountain glaciers.* International Hydrological Programme, Technical Documents in Hydrology (59). Paris: UNESCO, SC-2003/WS/4.

Knight, P.G., 1999. *Glaciers*. Cheltenham: Stanley Thornes Ltd, 261.

Kunaka, D., 2020. Factors Affecting Insolation & Temperature Variations around the Globe [online]. The Geo Room. Available from: https://thegeoroom.co.zw/climatology/factors-affecting-insolation-temperature-variations-around-the-globe/ [Accessed 30th April 2023].

Kurtz, D., 2013. *Kenai Fjords Resource Brief: Glacier Mass Balance*. National Park Service, U.S. Department of the Interior.

Leroux, D., and Pellarin, T., 2016. *11 - Remote Sensing Data Assimilation: Applications to Catchment Hydrology, In: Land Surface Remote Sensing in Continental Hydrology* [online]. Elsevier, 363-399.

Li, Y., Ding, Y., Shangguan, D., Liu, F., and Zhao, Q., 2021. Climate-driven acceleration of glacier mass loss on global and regional scales during 1961–2016. *Science China Earth Sciences* [online], 64 (4), 589-599.

Linacre, E., and Geerts, B., 1999. Surface Temperature in Antarctica [online]. University of Wyoming. Available from: http://www-das.uwyo.edu/~geerts/cwx/notes/chap03/antarctica.html [Accessed 30th April 2023].

Liu, X., 2008. Airborne LiDAR for DEM generation: some critical issues. *Progress in Physical Geography* [online], 32 (1), 31-49.

Liu, X., 2016. *Chapter 3 - Linear mixed-effects models in Methods and Applications of Longitudinal Data Analysis* [online]. Academic Press: Elsevier, 61-94.

Lundesgaard, O., Sutherland, D., Truffer, M., Pwell, B., Merrifield, M.A., and Winsor, P., 2018. *Glacier-Ocean Interactions in Western Antarctic Peninsula Fjords, In: AGU Fall Meetings Abstracts (C21C)* [online], 1341.

Marešová, J., Gdulová, K., Pracná, P., and Moravec, D., 2021. Applicability of Data Acquisition Characteristics to the Identification of Local Artefacts in Global Digital Elevation Models: Comparison of the Copernicus and TanDEM-X DEMs. *Remote Sensing* [online], 13 (3931).

Meier, M.F., Dyurgerov, M.B., Rick, U.K., O'neel, S., Pfeffer, W.T., Anderson, R.S., Anderson, S.P., and Glazovsky., 2007. Glaciers dominate eustatic sea-level rise in the 21st century. *Science* [online], 317 (5841), 1064-1067.

Meier, M.F., 2022. *Ice* [online]. Britannica. Available from: https://www.britannica.com/science/ice [Accessed 9th December 2022].

Moholdt, G., Heid, T., Benham, T., and Dowdeswell, A., 2017. Dynamic instability of marine-terminating glacier basins of Academy of Sciences Ice Cap, Russian High Arctic. *Annals of Glaciology* [online], 56 (60), 193-201.

Nesje, A., 2014., *Reference Module in Earth Systems and Environmental Sciences: Reconstructing Paleo ELAs on Glaciated Landscape.* Elsevier.

National Aeronautics and Space Administration (NASA)., 2022. *Antarctica mass variation since 2002* [online]. California: NASA. Available from: https://climate.nasa.gov/vital-signs/ice-sheets/ [Accessed 23rd December 2022].

National Aeronautics and Space Administration (NASA)., 2023. Interferometry [online]. Available from: https://nisar.jpl.nasa.gov/mission/get-to-know-sar/interferometry/ [Accessed 21st April 2023].

National Air and Space Museum., 2023. *Camera, Aerial, Fairchild K-17C* [online]. Washington. Available from: https://airandspace.si.edu/collection-objects/camera-aerial-fairchild-k-17c/nasm_A19970538000 [Accessed 26th January 2023].

National Oceanic and Atmospheric Administration (NOAA)., 2023. *What is lidar?* [online]. National Ocean Service. Available from: https://oceanservice.noaa.gov/facts/lidar.html [Accessed 15th April 2023].

National Snow and Ice Data Centre (NSIDC)., 2022. *World Glacier Inventory: Antarctica* [online]. Available from: https://nsidc.org/data/glacier_inventory/antarctica.html [Accessed 10th October 2022].

Niculiță, M., Mărgărint, M.C., and Tarolli, P., 2020. Chapter 10 - Using UAV and LiDAR data for gully geomorphic changes monitoring. *Developments in Earth Surface Processes* [online], 23, 271-315.

Oraschewski, F.M., and Grinsted, A., 2022. Modelling enhanced firn densification due to strain softening. *The Cryosphere* [online], 16 (7), 2683-2700.

Osmaston, H., 2005. Estimates of glacier equilibrium line altitudes by the Area Altitude, the Area Altitude Balance Ratio and the Area Altitude Balance Index methods and their validation. *Quaternary International*, 138-139, 22-32.

Papworth, H.E., 2014. *An assessment of archive stereo-aerial photographs for 3-dimensional reconstruction of damaged and destroyed archaeological earthworks.* Bournemouth: Bournemouth University.

Pasik, M., Bakula, K., Rozycki, S., Ostrowski, W., Kowalska, M.E., Fijalkowska, A., Rajner, M., Lapinski, S., Sobota, I., and Kejna, M., 2021. Glacier Geometry Changes in the Western Shore of Admiralty Bay, King George Island over the Last Decades. *Sensors* [online], 21 (4), 20210223.

Parks, C., 2022. *Glacier* [online]. National Geographic Society. Available from: https://education.nationalgeographic.org/resource/glacier [Accessed 29th December 2022].

Pelt, W.J.J., Pohjola, V.A., and Reijmer, C.H., 2016. The Changing Impact of Snow Conditions and Refreezing on the Mass Balance of an Idealized Svalbard Glacier. *Frontiers in Earth Science* [online], 4.

Pineda-Metz, S.E.A., 2021. Blue carbon pathways in West Antarctic fjords. *Global Change Biology* [online], 28, 8-20.

Pudelko, R., Angiel, P.J., Potocki, M., Jedrejek, A., and Kozak, M., 2018. Fluctuation of Glacial Retreat Rates in the Eastern Part of Warszawa Icefield, King George Island, Antarctica, 1979-2018. *Remote Sensing* [online], 10 (6), 892.

Pulighe, G., and Fava, F., 2013. DEM extraction from archive aerial photos: accuracy assessment in areas of complex topography. *European Journal of Remote Sensing* [online], 46 (1), 363-378.

Rau, F., Mauz, F., Vogt, S., Khalsa, S.J.S., and Raup, B., 2005. *Illustrated GLIMS Glacier Classification Manual: Glacier Classification Guidance for the GLIMS Glacier Inventory* (Version 1.0) [online]. GLIMS Regional Center 'Antarctic Peninsula'.

Rignot, E., and Thomas, R.H., 2002. Mass Balance of Polar Ice Sheets. *Science* [online]. 297 (5586), 1502-1506.

Rignot, E., 2006. Changes in ice dynamics and mass balance of the Antarctic ice sheet. *Philosophical Transactions of The Royal Society A: Mathematical, Physical and Engineering Sciences* [online], 364 (1844).

Rott, H., Rack, W., Skvarca, P., and Angelis, H.D., 2002. Northern Larsen Ice Shelf, Antarctica: further retreat after collapse. *Annals of Glaciology* [online], 34, 277-282.

Ruzgiene, B., and Alekniene, E., 2012. Analytical and digital photogrammetric geodata production systems (a comparison test). *Geodezija ir Kartografija* [online], 30 (2), 50-54.

Satsense., 2021. *LiDAR vs InSAR* [online]. Satsence. Available from: https://satsense.com/news/lidar-vs-insar [Accessed 26th April 2023].

Scambos, T.A., Hulbe, C.L., Fahnestock, M., and Bohlander, J., 2000 The link between climate warming and break up of ice shelves in the Antarctic Peninsula. *Journal of Glaciology* [online], 46, 516–530.

Scambos, T., Berthier, E., Haran, T., and Shuman, C.A., 2014. Detailed ice loss pattern in the northern Antarctic Peninsula: Widespread decline driven by ice front retreats. *The Cryosphere* [online], 8 (3), 3237-3261.

Seehaus, T., Cook, A.J., Silva, A.B., and Braun, M., 2018. Changes in glacier dynamics in the northern Antarctic Peninsula since 1985. *The Cryosphere* [online], 12 (2), 577-594.

Seehaus, T., 2021. *Mid-Term Report: Mass balance and ice dynamics of Antarctic Peninsula glaciers, MIT-AP*. Germany: Friedrich-Alexander-Universität Erlangen-Nürnberg, Institute of Geography.

Shepherd, A., Wingham, D., Payne, T., and Skvarca, P., 2003. Larsen Ice Shelf has progressively thinned. *Science* [online], 302, 856–859.

Simmon, R., 2007. *Two Decades of Temperature Change in Antarctica (1981-2007)* [online]. NASA Earth Observatory. Available from: https://web.archive.org/web/20080920041805/http://earthobservatory.nasa.gov/Newsroom/NewImages/images.php3?img_id=17838 [Accessed 2nd May 2023].

Sivapal., 2016. *The Life and Work of Louis Agassiz* [online]. University of Illinois Urbana-Champaign. Available from: https://publish.illinois.edu/louisagassiz/ice-ages/ [Accessed 14th March 2023].

Stanhill, G., and Cohen, S., 1997. Recent Changes in Solar Irradiance in Antarctica. *Journal of Climate* [online], 10 (8), 2078-2086.

Steiner. D., Zumbühl H.J., and Bauder. A., 2007. *Two Alpine glaciers over the last two centuries: a scientific view based on pictorial sources. In: Orlove, B., Wiegandt, E., and B. Luckman.., The DarkeningPeaks: Glacial Retreat in Scientific and Social Context.* Berkeley: University of California Press.

Swedish National Heritage Board., 2019. *Equipment and procedures for photogrammetry* [online]. Tillgänglighet: Swedish National Heritage Board. Available from: https://www.raa.se/in-english/outreach-and-exhibitions/guide-for-publishing-3d-models/equipment-and-procedures-for-photogrammetry/ [Accessed 7th November 2022].

Thomas, E.R., Marshall, G.J., and McConnell, J.R., 2008. A doubling in snow accumulation in the western Antarctic Peninsula since 1850. *Geophysical Research Letters* [online], 35 (1).

Thomas, E.R., Melchior van Wessem, J., Robers, J., Isaksson, E., Schlosser, E., Fudge, T.J., Vallelonga, P., Medley, B., Lenaerts, J., Bertler, N., van den Broeke, M.R., Dixon, D.A., Frezzotti, M., Stenni, B., Curran, M., and Ekaykin, A.A., 2017. Regional Antarctic snow accumulation over the past 1000 year. *Climate of the Past,* 13, 1491-1513.

Thompson, L.G., Brecher, H.H., Mosley-Thompson, E., Hardy, D.R., and Mark, B.G., 2009. Glacier loss on Kilimanjaro continues unabated. *PNAS Earth, Atmospheric, and Planetary Science* [online], 106 (47), 19770-19775.

Tintaly., 2023. *Tinitaly DEM* [online]. Istituto Nazionale di Geofisica e Vulcanologia. Available from: https://tinitaly.pi.ingv.it/ [Accessed 26th April 2023].

Turner, J., Colwell, S.R., Marshall, G.J., Lachlan-Cope, T.A., Carleton, A.M., Jones, P D., Lagun, V., Reid, P. A., and Iagovkina, S., 2005. Antarctic climate change during the last 50 years. *International Journal of Climatology* [online], 25(3), 279-294.

Turner, J., Marshall, G.J., Clem, K., Colwell, S., Phillips, T., and Lu, H., 2020. Antarctic temperature variability and change from station data. *International Journal of Climatology* [online], 40 (6), 2986-3007.

World Topographic Map., 2023. *Antarctic Peninsula topographic map* [online]. Topographic Map. Available from: Antarctic Peninsula topographic map, elevation, terrain (topographic-map.com) [Accessed 19th March 2023].

United States Geological Survey (USGS)., 2023. *To Determine Percent of Slope and Angle of Slope* [online]. Educational Resources, USGS. Available from: https://www.usgs.gov/educational-resources/determine-percent-slope-and-angle-slope [Accessed 28th April 2023].

VanLooy, J., Forster, R., and Ford, A., 2006. Accelerating thinning of Kenai Peninsula glaciers, Alaska. *Geophysical Research Letters,* 33, L21307.

Vaughan, D.G., Marshall, G.J., Connolley, W.M., King, J.C. and Mulvaney, R., 2001. The devils in the details. *Science* [online], 293, 1777–1778.

Volksen, C., and Mayer, C., 2016. *Monitoring the Dynamics of Glaciers with Low-Cost GNSS receivers* [PowerPoint]. Bavarian Academy of Sciences and Humanities: Germany.

West, G., and Howard, R., 2019. *UBC ATSC 113 - Weather for Sailing, Flying & Snow Sports: 7h Aspect Effects* [online]. The University of British Columbia, Department of Earth, Ocean and Atmospheric Sciences. Available from: https://www.eoas.ubc.ca/courses/atsc113/snow/met_concepts/07-met_concepts/07h-aspect-effects/ [Accessed 30th April 2023].

Williams, R.S., and Ferrigno, J.G., 2005. *Satellite Image Atlas of Glaciers of The World*. United States Geological Survey Professional Paper, 1386–A–2.

Zachariah, J. V., 2019. *Understanding Photogrammetry* [online]. Medium. Available from: https://joelvzach.medium.com/understanding-photogrammetry-7b8867b072a4 [Accessed 3rd November 2022].

Zemp, M., Huss, M., Thibert, E., Eckert, N., McNabb, R., Huber, J., Barandun, M., Machguth, H., Nussbaumer, S.U., Gartner-Roer, I., Thomson, I., Paul, F., Maussion, F., Kutuzov, S., and Cogley, J.G., 2019. Global glacier mass changes and their contributions to sea-level rise from 1961 to 2016. *Nature* [online], 568, 382-386.

Zeng, Z., Wang, X., Wang, Z., Zhang, W., Zhang, D., Zhu, K., Mai, X., Cheng, W., and Ding, M., 2022. A 35-year daily global solar radiation dataset reconstruction at the Great Wall Station, Antarctica: First results and comparison with ERA5, CRA40 reanalysis, and ICDR (AVHRR) satellite products. *Frontiers in Earth Science: Environmental Informatics and Remote Sensing* [online], 10.

9.0 Appendix: Learning Contract and Interim comments

BU Bournemouth University

LEARNING CONTRACT: INDEPENDENT RESEARCH PROJECT

The learning contract is an agreement between student and supervisor: it should clearly indicate what is expected from both sides. The text in Sections 2 and 3 provides guidance and can be modified to give more details reflecting what has been agreed, such as deadlines for submission of drafts and provision of feedback, word count limits/exclusions and number/timing of meetings.

Importantly, the document checklist helps students to follow the required procedures (e.g. ethical approval and risk assessment) and communicate what has been done to the supervisor.

The student should submit a draft of the completed form to the supervisor and request a meeting to discuss and finalise the content. Both the student and the supervisor are responsible for keeping a signed copy of this document and following what has been mutually agreed.

1. YOUR DETAILS

Student name: Evangeline Rowe

Degree Programme: BSc Environmental Science

Proposed IRP Title or Set Project: Measuring Decadal Changes in Glacier Thickness using Aerial Photography

Supervisor name: Andy Ford

2. As the student undertaking the above project I agree to:

- E-mail my supervisor on a fortnightly basis with a progress report
- Meet with my supervisor at least once a month to discuss progress and I understand that it is my responsibility to organise these meetings
- Comply with the terms of this learning contract and the guidance set out in the Guide to Independent Research Projects
- I understand that this is an *independent* project and that I am solely responsible for its completion
- I agree to comply with all ethical, laboratory and fieldwork protocols established by the Faculty.

3. As the supervisor of this project I agree to:

- Meet with the student undertaking this project on at least a monthly basis and to respond to the progress e-mails as appropriate
- To meet formally with the student during the first week in November to undertake the interim interview
- To provide guidance and support to the student undertaking this project bearing in mind that it is an *independent* research project. This is inclusive of commenting on drafts of the final report in a timely fashion.

3. DOCUMENT CHECKLIST

Research Proposal or Plan Attached? ☐ YES ☑ NO

☐ YES	☑ NO	**Risk Assessment for fieldwork and evidence of COSSH assessment for all laboratory procedures (online risk assessment completed)**
☐ YES	☑ NO	**Completed booking for all field equipment**
☐ YES	☑ NO	**Letters of permission where appropriate providing evidence of access to such things as field sites and/or museum archives**
☐ YES	☑ NO	**Completed Ethics Checklist**

4. INTERIM INTERVIEW – Progress evaluation

1. Read and make notes regarding glacial mass balance.
2. Read and make takes regarding methods of observing mass balance. Including advantages, disadvantages, and any gaps in knowledge.
3. Read and make notes regarding the development of photogrammetry over time, early hardware and how software has and is being used across all fields.
4. Read and make notes regarding the use of photogrammetry in glaciology. Its advantages, disadvantages, and any gaps in knowledge.
5. Read and make notes regarding how photogrammetry works in theory.
6. Read and make notes regarding how photogrammetry works in practice.
7. Complete a 200-word introduction regarding the mass balance and the use of photogrammetry.
8. Decided on which glaciers to focus research on.
9. Short list the available data on chosen glaciers.
10. Write a research question.

Interim Review Date: 29/11/2022

5. Variance from the Independent Research Project Guide

The IRP assessment is normally governed by the guidance provided in the Independent Research Project Guide. Any variance in terms of format (e.g. technical report, scientific paper) and word limit

should be agreed and specified here. Submission date cannot be changed unless evidence of mitigating circumstances is provided in accordance with the standard BU Guidelines.

Any changes? ☐ **YES** ☑ **NO** If YES please provide details below:

Both of the undersigned parties agree to be bound by this learning contract:	
Student Signature:	
PRINT NAME:	EVANGELINE ROWE
Date:	03/11/2022

Supervisor Signature:	
PRINT NAME:	ANDREW FORD
Date:	3/11/22